Gregory F. Nellis, Assistant Professor - University of Wisconsin - Madison

Approved: _____ *Date*: 12/9/04

John M. Pfotenhauer, Associate Professor - University of Wisconsin - Madison

Approved: _____ *Date*: 12/9/04

Experimental Measurement of Heat Transfer Coefficients for Mixed Gas Working Fluids in Joule-Thompson Systems

By

Cory B Hughes

A thesis submitted in partial fulfillment of
the requirements for the degree of

MASTERS OF SCIENCE
(Mechanical Engineering)

UNIVERSITY OF WISCONISN – MADISON
2004

Experimental Measurement of Heat Transfer Coefficients for Mixed Gas Working Fluids in Joule-Thompson Systems

Cory B Hughes, M.S.
Department of Mechanical Engineering
University of Wisconsin–Madison, 2004
Professor John Pfotenhauer, Advisor
Professor Greg Nellis, Advisor

The use of non-azeotropic hydrocarbon mixtures in throttle-cycle refrigeration systems has resulted in large increases in the performance of Joule-Thomson type cryocoolers. However, there are very few data and inadequate theory currently available in the literature regarding the thermal-fluid behavior of multi-component, multi-phase mixtures at cryogenic temperatures. The design of these systems is therefore semi-empirical, relying heavily on experimental iteration. In this work, an experimental apparatus is described that is capable of making precise and controlled measurements of the heat transfer coefficient over a range of cryogenic temperatures, compositions, geometries, and flow rates that are relevant to small-scale, throttle-cycle refrigeration systems.

The experimental apparatus is used to carry out a study of the horizontal flow boiling heat transfer coefficient for a non-azeotropic hydrocarbon mixture in a circular cross-section with a constant wall temperature. The measurements are carried out over a range of cryogenic temperatures and the data are presented in the form of heat transfer coefficients as a function of temperature and thermodynamic quality. The experimental uncertainty of the measurements is theoretically estimated to be 10%. Measurements of the single-phase heat transfer coefficient for pure nitrogen fall within 10% of the Dittus-Boelter correlation.

Acknowledgments

I would first like to thank my advisors Dr. John Pfotenhauer and Dr. Greg Nellis for all their patience and support; and the Office of Naval Research for providing the funding for this work.

Beyond this I would like to send out a big thank you to all my family and friends that have kept me from running off to Mexico to work in a biker bar: my folks Barry and Elizabeth Hughes; the McFarland Clan: Mac-D, Sharon, Maureen and soon to be little Daniel; my brother Jesse, his wife Amy, and my beautiful niece Eva; my special lady Holly for her deep understanding of my lack of common sense; Alex Dodd and his knack for sleepless nights with the Gas Chromatograph; Dr. Joe Musto and the Mechanical Engineering faculty at the Milwaukee School of Engineer for their inspiration and friendship; and everyone here at the Solar Energy Lab that has made my experience in Madison, Wisconsin one that will bring a smile to my face for years to come.

Table of Contents

List of Tables

List of Figures

Nomenclature

Symbol	Description	Units
A_s	test section inner surface area	m^2
C	concentration	mol %
c	thermal capacitance	J/K
c_P	specific heat capacity at constant pressure	J/kg-K
D_c	Outer diameter of cryocooler cold head	m
D_i	test section inner diameter	m
E	constant in the Stephan-Abdelsalam correlation	
h	enthalpy	J/kg-K
htc	heat transfer coefficient	W/m^2-K
I	current	amp
k	thermal conductivity	W/m-K
L	heated length	m
L_{block}	length of cryocooler cold head	m
$\dot{m}$	mass flow rate	kg/s
n	constant in the Stephan-Abdelsalam correlation	
P	pressure	Pa
$\dot{q}$	heat transfer rate	W
$\dot{q}''$	heat flux	W/m^2
ρ	density	kg/m^3
R	thermal resistance	K/W
T	temperature	K
T_1	test section inlet temperature	K
T_2	test section exit temperature	K
T_b	isothermal test section temperature	K
V	voltage	V
ΔT	stream-to-stream temperature difference	K
ΔT_g	temperature glide	K
ΔT_{lm}	log mean temperature difference	K
δ	uncertainty of a quantity	
τ	time constant	s^{-1}

Subscripts

Symbol	Description
1^{st}	first redundant temperature sensor
2^{nd}	second redundant temperature sensor
high	high pressure
i	inner
in	inlet
load	refrigeration load
low	low pressure
out	outlet
w	wall
b	copper test section block

1.0 Introduction

1.1 Mixed Gas JT Cooling

Figure 1.1 shows the schematic of the Joule-Thompson (JT) refrigeration cycle and Figure 1.2 shows the cycle on a temperature-entropy diagram. The working fluid is compressed and then passes through an aftercooler where its temperature is reduced to near room temperature, state (3). The working fluid passes through a recuperative heat exchanger where it is pre-cooled to cryogenic temperatures. The high pressure, cold refrigerant, state (4) is expanded through a valve to state (5). The isenthalpic expansion causes a temperature drop and the low pressure fluid can accept some refrigeration load before it re-enters the recuperator at state (6).

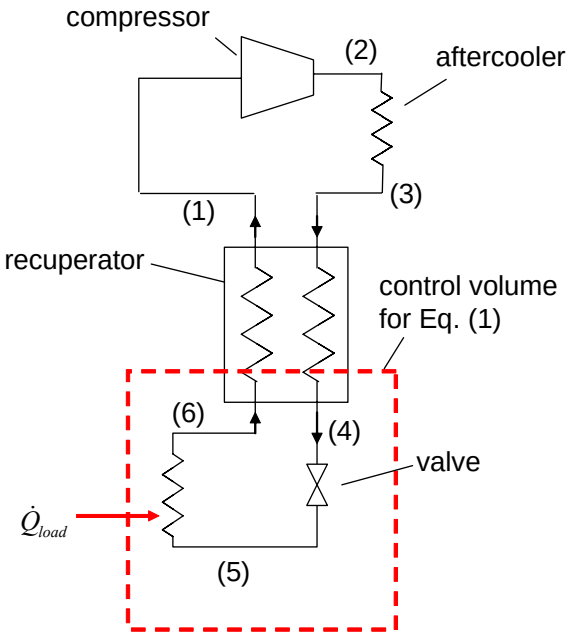

Figure 1.1. Schematic of a JT refrigerator

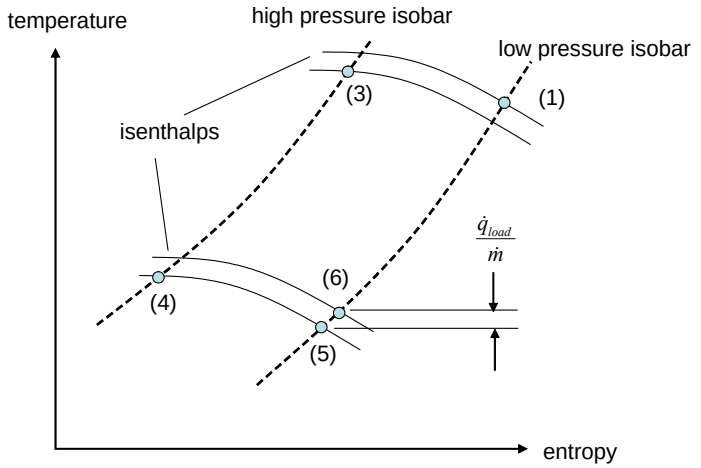

Figure 1.2. Temperature-entropy diagram of a JT cycle

The simplicity of the cycle leads to reliability and low cost and therefore the JT cycle is attractive for many applications, including cooling of sensors (Rijpma et al. 2003), biomedical samples, and cryosurgical probes (Naer 2002). However, the efficiency of the Joule-Thomson cycle is fundamentally limited by the properties of the working fluid in a way that other refrigeration cycles are not. An energy balance that encompasses the cold end of the JT cycle and passes through the heat exchanger at an arbitrary location (see dashed line in Figure 1.1) reveals that the energy associated with the refrigeration load ($\dot{Q}_{load}$) is transferred as an enthalpy flux related to the difference in enthalpy between the low pressure gas returning to the compressor and the high pressure gas supplied to the cold end:

$$\dot{Q}_{load} = \dot{m}\left[h\left(P_{low}, T\right) - h\left(P_{high}, T + \Delta T\right)\right] \tag{1.1}$$

where h is enthalpy, $\dot{m}$ is the mass flow rate, P_{low} and P_{high} are the low and high pressures driving the cycle, respectively, T is the local temperature, and ΔT is the stream-to-stream temperature difference driving the heat transfer. Equation 1.1 implies that the maximum refrigeration load is defined by the minimum enthalpy difference between the low and

high pressure streams exhibited by the working fluid over the temperature range spanned by the recuperative heat exchanger. The refrigeration capacity is therefore extremely dependent upon the thermodynamic properties of the working fluid; specifically the real gas properties of the fluid must be large over a large temperature range. Pure substances tend to exhibit significant real gas effects only in a narrow temperature range close to the vapor dome. However, non-azeotropic refrigerant mixtures have a much broader vapor dome and therefore exhibit significant real gas effects over a much larger temperature range. Therefore, these refrigerants can increase the minimum enthalpy difference between the low and high pressure fluid streams and thus the performance of the JT cycle. The use of gas mixtures as working fluids in JT systems have substantially increased their performance. As a typical example, Alfeev et al. (1973) increased the cooling capacity of a pure nitrogen system by approximately an order of magnitude using a hydrocarbon mixture.

1.2 Active Cooling of Current Leads

One application of a mixed gas JT system is as a means for cooling electrical leads for a high-temperature superconducting electronics package. By integrating the leads, which are resistive and therefore present both a conductive and dissipative load on the system, directly with the recuperative heat exchanger in the JT system it is possible to intercept some of the refrigeration load at a high temperature where it represents the smallest entropy flow. A significant thermodynamic advantage is obtained in this configuration.

The design of these mixed gas JT systems is currently limited by a lack of generally applicable data or theory that allows accurate prediction of the forced heat transfer coefficient for a multi-phase, multi-component fluid.

1.3 Heat Transfer Coefficient Measurement Techniques

The heat transfer coefficient that characterizes the convective heat transfer between a flow of gas and the wall of a channel can be measured by passing a controlled flow of fluid through a heated, or cooled, channel of known dimensions, and measuring the local temperature of the fluid channel wall, the fluid bulk temperature, and the applied heat load (or cooling load). The flow can pass through multiple channels or a single channel of various sizes and shapes. Experiments measuring heat transfer coefficient can be categorized based on the thermal boundary condition at the channel wall: constant heat flux, constant wall temperature, or interaction with a secondary heat transfer fluid.

A constant heat flux or constant wall temperature boundary condition can be approximately generated using an electrical heater wound around either a non-conductive or highly conductive wall, respectively, or an electrical current is passed directly through the channel wall (Jung 1989). In these cases, the applied heat load can be measured directly. A constant temperature boundary condition can also be obtained via the phase change of a single component fluid over the external channel wall.

When the heat load is applied via interaction with a secondary heat transfer fluid, the flow is ordinarily arranged in a counterflow tube-in-tube type heat exchanger arrangement (Kattan 1998). The applied heating load in this method is determined indirectly using an energy balance on the secondary heat transfer fluid as it passes through the heat exchanger. The experimental apparatus in this example consists of instrumented sections of tube-in-tube style heat exchangers. The temperature of the tube

wall is measured, the temperature of the fluid is determined from either an analytically or numerically generated fluid temperature profile, and the applied heat determined from an energy balance of the heat transfer fluid across the test sections. This method of heat transfer coefficient measurement produces more of an average heat transfer coefficient as opposed to local heat transfer coefficients that can be measured using the previous two methods.

Currently, the average overall heat transfer coefficient has been measured for mixed gas cryogenic refrigerants using the heat exchanger type measurement method. Boiarski et al. (1999) has measured overall heat transfer coefficients of a mixed gas cryogenic refrigerant from the inlet and outlet temperatures of a recuperative heat exchanger in a mixed gas JT cycle. Gong (2001) has measured the overall heat transfer coefficient of a mixed gas cryogenic refrigerant for a range of temperatures and compositions using instrumented sections of a tube-in-tube heat exchanger. However, an averaged heat transfer coefficient does not provide the detailed information necessary to understand the complex behavior of a two-phase non-azetropic mixture. Local heat transfer coefficient measurements are essential for development of recuperative heat exchangers in mixed gas JT cycles. This work presents the design and development of a test facility that has been used to accurately measure the local heat transfer coefficient for mixed refrigerants at cryogenic temperatures and test conditions that reflect those of a compact recuperative heat exchanger.

1.4 Heat Transfer of Multi-phase Mixed Gas

As a result of the complex transport mechanisms involved in flow boiling for a mixture there is currently no adequate theory to describe the process. The two-phase flow regime is the single most important factor in the prediction of heat transfer coefficient. Flow regimes are best described graphically with a flow map, as shown in Figure 1.3 for an air/water flow through a 1 mm ID glass tube (Damianides, 1988).

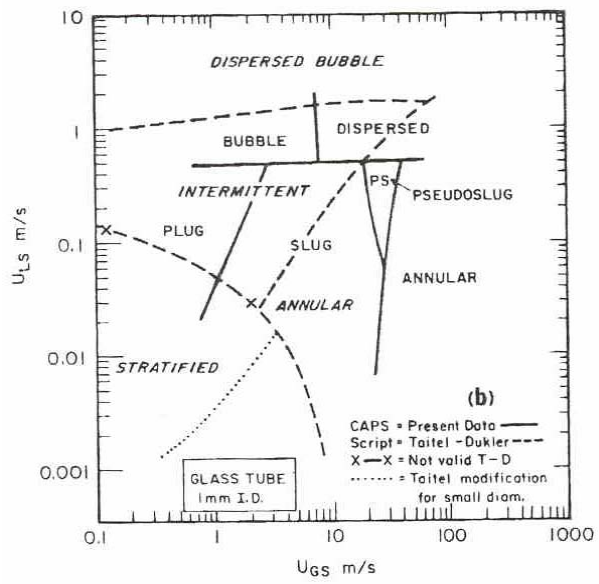

Figure 1.3. Flow map of an air/water mixture in a 1mm ID glass tube, from Damianides (1988)

For a small diameter channel, the majority of the area of the flow map is taken up by the annular and slug flow regimes that are characterized by the presence of a liquid film on the entire perimeter of the tube. The ability to wet the perimeter early and delay the onset of dry-out increases the heat transfer coefficient in capillary tubes. Zhao (2001) presents heat transfer coefficient data that is essentially independent of mass flux, suggesting the dominance of nucleate boiling heat transfer. Wambsganss (1993) also presents heat

transfer coefficient data for small diameter tubes that suggests that nucleate boiling dominates the process.

The design of the heat transfer test facility is described in the next section. In order to design for the desired level of accuracy, it is important to obtain some estimate of the heat transfer coefficient prior to its measurement. The type of instrumentation, length of the test section, and level of heat transfer are all contingent upon the magnitude of the heat transfer coefficient that is expected.

Wambsganss (1993) compares nine different, commonly used flow boiling correlations with his experimental data and reports that the Stephan-Abdelsalam correlation (1978) for natural convection pool boiling predicts the heat transfer coefficient in small diameter tubes better than all but the Lazarek and Black (1982) flow boiling correlation. The Lazarek and Black correlation is a flow boiling correlation that balances nucleate boiling and convective boiling heat transfer and predicts the heat transfer coefficient data for small diameter tubes by heavily weighting the nucleate boiling term so that it coincides with trends observed from data. The Stephan-Abdelsalam correlation is a pool boiling correlation, and therefore predicts only the heat transfer coefficient (*htc*) due to nucleate boiling. The Stephan-Abdelsalam correlation has the form:

$$htc = E\left(\dot{q}''\right)^n \tag{1.2}$$

where $\dot{q}''$ is the heat flux, and the constants E and n are based on fluid properties and experimental data. The simple form of this correlation outweighs the marginal loss of accuracy; Wambsganss found that the Lazarek and Black correlation predicted 84.8% of

the data to within ±20%, whereas the Stephan-Abdelsalam predicted 83.8% of the data to within ±20%. Based on this result, the Stephan-Abdelsalam correlation is used to estimate the heat transfer coefficient in order to proceed with the design of this experiment, as described in the subsequent chapter.

During a constant pressure phase change, a mixture experiences a change in temperature, known as a temperature glide. Figure 1.4 shows a phase diagram for an arbitrary binary mixture. The concentration of the more volatile component, B, is shown on the x-axis and temperature is shown on the y-axis.

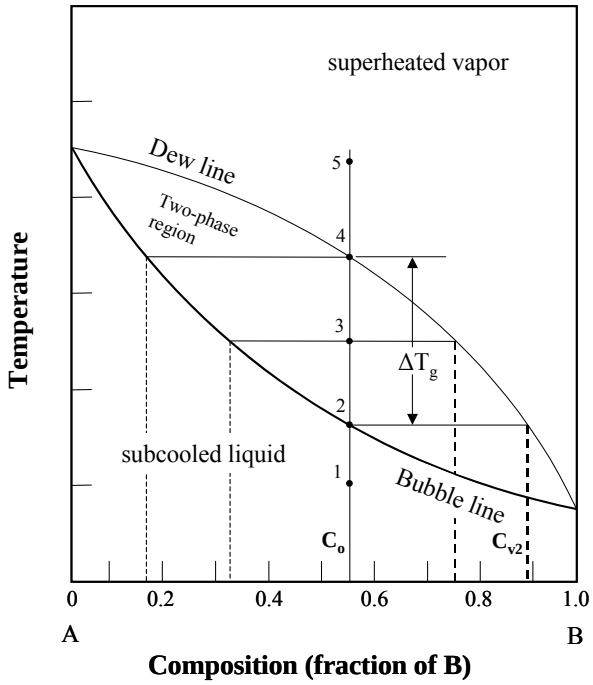

Figure 1.4. Phase Diagram for a Binary Mixture

The progression of a mixture through the evaporation process is represented by the vertical line in Figure 1.4. At point (1), the mixture is all liquid, and has a composition, C_o. At point (2) the evaporation process is initiated and the vapor that is produced has concentration of C_{v2}. At point (2), the vapor phase has the greatest concentration of the

more volatile component. As the quality increases, the liquid phase becomes richer in the less volatile component, and the concentration of the more volatile component in the vapor phase decreases. As the liquid phase becomes richer in the less volatile component, the superheat required to nucleate the vapor phase increases. The evaporation process does not occur at constant temperature as it would in a pure substance, instead a temperature glide, ΔT_g, results as described by Jung et al. (1989). The concentration gradient between the liquid and the vapor suppresses nucleate boiling by creating diffusive mass fluxes; as a result, correlations developed for pure fluids are not generally applicable for mixtures.

2.0 Test Facility Design

2.1 Experimental Design

2.1.1 Measurement Concept

The objective of this experiment is to introduce a flow of a gas mixture with controlled temperature, pressure, and composition into a constant wall temperature section of tube where heat is added, as shown in Figure 2.1.

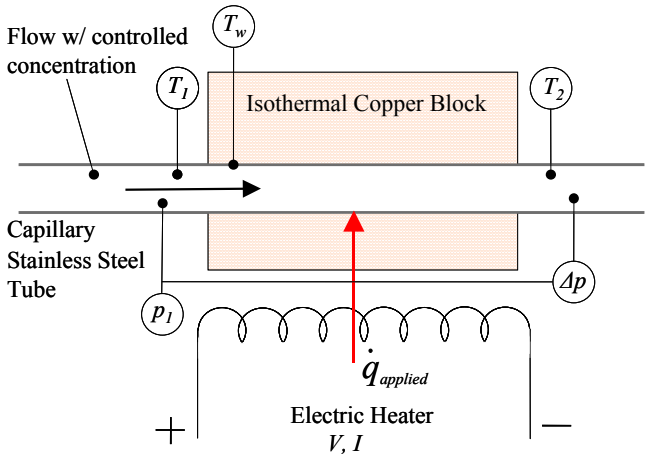

Figure 2.1. Conceptual diagram of the test section used to measure heat transfer coefficient.

The heat transfer coefficient (*htc*) is determined by measuring the electric power supplied to the heater ($\dot{q}_{applied}$),the fluid temperature at the inlet (T_1) and exit (T_2) of the section, and the block temperature (T_b) that is related to the temperature of the wall of the test section (T_w). These temperatures are sufficient to determine the log mean temperature difference (ΔT_{lm}) between the fluid and the wall. The heat transfer coefficient is defined by Eq. 2.1.

$$\dot{q}_{applied} = htc\ A_s\ \Delta T_{lm} \tag{2.1}$$

where A_s is the inside surface area of the heated tube length, given by:

$$A_s = \pi D_i L \tag{2.2}$$

and D_i and L are the inner diameter and length of the test section, respectively. The log mean temperature difference, ΔT_{lm}, is given by:

$$\Delta T_{lm} = \frac{\Delta T_1 - \Delta T_2}{\ln\left(\frac{\Delta T_1}{\Delta T_2}\right)} \tag{2.3}$$

where:

$$\Delta T_1 = T_w - T_1 \tag{2.4}$$

and

$$\Delta T_2 = T_w - T_2 \tag{2.5}$$

Equations 2.3 through 2.5 imply that there is no temperature difference between the copper block (T_b) and the inner surface of the tube (T_w). This assumption will be evaluated and corrected in subsequent sections.

2.1.2 Target Test Conditions

The target test conditions are listed in Table 2.1. These conditions were based on typical dimensions and operating parameters of a small scale Joule-Thompson cycle cryocooler. The fluid mixture composition is determined from an optimization method developed by Keppler et al. (2004) to maximize the UA per unit mass flow rate of a JT cycle operating at specific cold temperature and pressure ratio. The target test conditions listed in Table 2.1 are representative but not comprehensive; the test facility will be capable of making measurements over a wide range of conditions. However, these conditions provide a meaningful basis to use for the experimental design process described in the subsequent sections.

Table 2.1. Target Test Conditions

Parameter		**Symbol**	**Target Value**
Mass flow rate		$\dot{m}$	0.6 g/s
Tube inner diameter		D_i	0.80 mm
Fluid inlet temperature		T_{in}	90 K*
Fluid inlet pressure		P_{in}	150 kPa to 1500 kPa
Fluid Composition	Nitrogen		21.60%
	Methane		31.3%
	Ethane		6.9%
	Propane		40.3%
	Isobutane		0.0%
Uncertainty in heat transfer coef.		δhtc	<10%

* the temperature range from 90 K to room temperature is considered

2.1.3 Instrumentation

Platinum resistive thermometers (PRTs) are used to measure all temperatures in the test facility. A two-point calibration (with liquid nitrogen and an ice bath) of each PRT provides an uncertainty of ±0.25 K (Lakeshore 2004). Redundant PRTs are mounted in the fluid stream at both the inlet and the outlet of the test section and are also used to measure the temperature of the copper block. The temperature measurements at each location (T_1, T_2, and T_b) represent an average of two PRT readings and therefore the uncertainty in the temperature measurements (δT) is reduced according to Eq. 2.6.

$$\delta T_1 = \sqrt{\left(\frac{1}{2}\delta T_{1,1st}\right)^2 + \left(\frac{1}{2}\delta T_{1,2nd}\right)^2} \tag{2.6}$$

where $T_{1,1st}$ and $T_{1,2nd}$ are the 1st and 2nd temperature measurements at the test section inlet. The uncertainty in T_1 is therefore reduced from its nominal value of ±0.25 K for a single temperature sensor to ±0.18 K. The same is true for δT_2 and δT_w.

The heat is applied to the test section electrically. The rate of heat transfer is determined by simultaneously measuring the voltage (V) and current (I) that is applied to the resistive heating element. The uncertainty of the current and voltage measurement is approximately 0.0015% of their readings. This level of uncertainty is significantly better than the uncertainty in the temperature measurements and therefore the effect of uncertainties in the current and voltage measurements are ignored.

2.1.4 Design of the Test Section

Solving Eq. (2.1) for the heat transfer coefficient illustrates that the uncertainty in the measured heat transfer coefficient depends directly on the uncertainty in the measurement of the heat load and the log mean temperature difference (assuming that the geometry is known exactly).

$$htc = \frac{\dot{q}_{applied}}{A_s \, \Delta T_{lm}} \tag{2.7}$$

As previously mentioned, uncertainty in the measurement of the applied load is considered negligible and the functional form of the heat transfer coefficient is therefore:

$$htc = htc\left(\Delta T_{lm}\right) \tag{2.8}$$

The uncertainty in the heat transfer coefficient (δhtc) is therefore:

$$\delta htc = \frac{\partial \, htc}{\partial \, \Delta T_{lm}} \delta \Delta T_{lm} = -\frac{\dot{q}_{applied}}{A_s \left(\Delta T_{lm}\right)^2} \delta \Delta T_{lm} \tag{2.9}$$

where:

$$\delta \Delta T_{lm} = \sqrt{\left(\frac{\partial \, \Delta T_{lm}}{\partial \, \Delta T_1} \delta \Delta T_1\right)^2 + \left(\frac{\partial \, \Delta T_{lm}}{\partial \, \Delta T_2} \delta \Delta T_2\right)^2} \tag{2.10}$$

and:

$$\frac{\partial \Delta T_{lm}}{\partial \Delta T_1} = \left[\frac{1}{\ln\left(\frac{\Delta T_1}{\Delta T_2}\right)} - \frac{\Delta T_1 - \Delta T_2}{\ln\left(\frac{\Delta T_1}{\Delta T_2}\right)^2 \Delta T_1} \right] \tag{2.11}$$

$$\frac{\partial \Delta T_{lm}}{\partial \Delta T_2} = \left[-\frac{1}{\ln\left(\frac{\Delta T_1}{\Delta T_2}\right)} + \frac{\Delta T_1 - \Delta T_2}{\ln\left(\frac{\Delta T_1}{\Delta T_2}\right)^2 \Delta T_2} \right] \tag{2.12}$$

where $\delta\Delta T_1$ and $\delta\Delta T_2$ are the uncertainties associated with the measured inlet fluid to wall and exit fluid to wall temperature differences, respectively. The uncertainty in the measured temperature difference is:

$$\delta\Delta T_1 = \sqrt{\left(-\delta T_1\right)^2 + \left(\delta T_w\right)^2} \tag{2.13}$$

and

$$\delta\Delta T_2 = \sqrt{\left(-\delta T_2\right)^2 + \left(\delta T_w\right)^2} \tag{2.14}$$

where δT_1, δT_2, and δT_w are the uncertainty of the temperature measurement at the inlet, exit, and wall of the test section, respectively and are equal to ±0.18 K. The resulting uncertainties in both measured temperature differences, $\delta\Delta T_1$ and $\delta\Delta T_2$, is ±0.25 K.

Figure 6 illustrates the fractional uncertainty in the heat transfer coefficient predicted using Equation 2.9 through 2.13 as a function of the heat load for various values of the test section length.

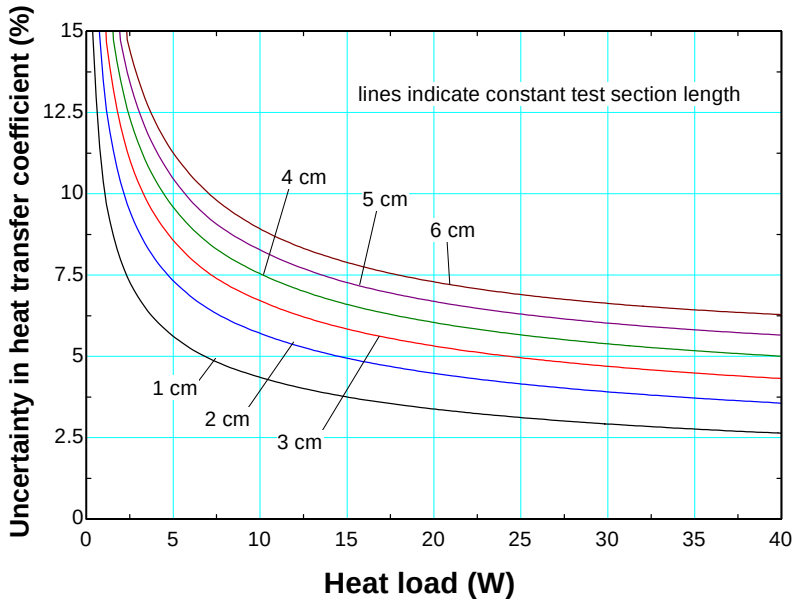

Figure 2.2. Theoretical uncertainty in the measured heat transfer coefficient as a function of heat load for various values of the test section length

Notice that the uncertainty in the heat transfer coefficient decreases with increasing heat load and decreasing test section length; both correspond to increasing fluid-to-wall temperature differences, which can therefore be measured more accurately. However, Figure 2.2 considers only one aspect of the uncertainty in the measurement. Larger heat loads will result in larger changes in the state of the fluid as it passes through the test section for a given mass flow rate. Large changes in the fluid properties are undesirable both because the use of the log mean temperature difference in Eq. (2.1) implies constant properties and also because a local measurement of the heat transfer is desired rather than a measurement that is averaged over a range of conditions. A more advanced, numerical approach that accounted for local changes in the fluid properties could replace the log mean temperature difference during data reduction, but at the expense of increasing complexity and uncertainty. The desire for a local measurement of the heat transfer coefficient is important due to the objective of providing more detailed, empirical data to

the lexicon of information regarding the heat transfer of multi-phase multi-component fluids.

Countering this is the fact that a smaller test section will correspond to a less well developed flow. The use of an adiabatic section of tube, 40 diameters in length, before the test ensures that the flow is nearly hydrodynamically developed, but thermal development still only occurs within the test section. Flow within a recuperative heat exchanger will be nearly fully developed over the entire length and therefore it is important that the bulk of the flow within the test section also be fully developed. A test section of 3.0 cm long provides an L/D_i ratio of nominally 37.

The variation of the fluid properties within the test section are evaluated by considering the maximum difference between the local and inlet properties; for example using the specific heat capacity:

$$\delta c_P = \frac{max\left(c_P\left(T, P_{in}\right) - c_P\left(T_{in}, P_{in}\right)\right)}{c_P\left(T_{in}, P_{in}\right)} \quad \text{evaluated from } T_{in} \text{ to } T_{out} \tag{2.15}$$

The fluid properties are evaluated using the NIST 4 Database (Ely, 2003). Figure 2.3 illustrates the fractional uncertainty in the specific heat capacity, density, and thermal conductivity as a function of heat load, evaluated at the target test conditions shown in Table 2.1. Note that the uncertainty in the fluid properties tends to increase with increasing heat load due to the larger induced change in the state of the fluid.

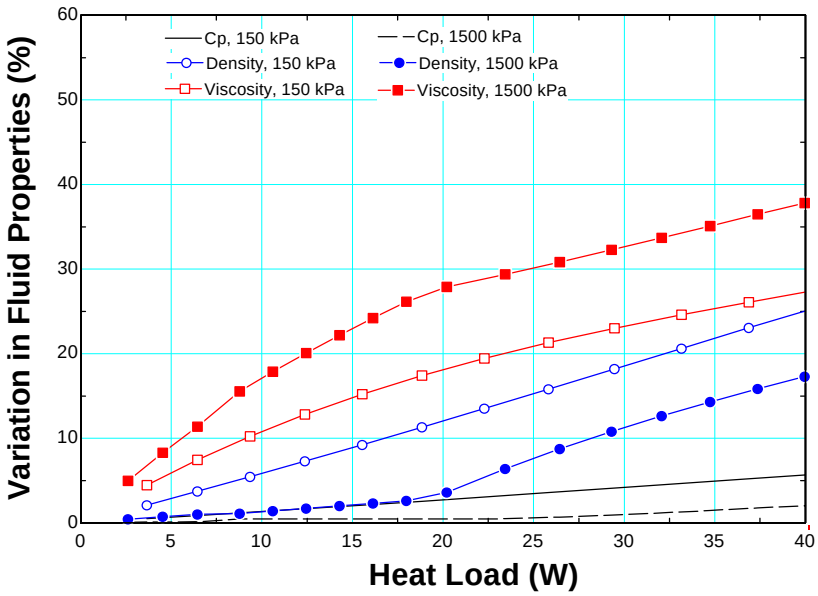

Figure 2.3. Fractional uncertainty in the specific heat capacity, density, and thermal conductivity as a function of the heat load at 90 K and various pressures

Figures 2.2 and 2.3 illustrate that an optimal heat load will balance the uncertainties in the measured log-mean temperature difference against variation in the fluid properties. The desired level of accuracy is <10% and this target can be met for most test conditions using a 3 cm long test section and a heat load of 5-10 W.

2.1.5 Other Test Section Design Issues

2.1.5.1 Uniformity of wall temperature

A relatively large cylindrical piece of copper is joined to the stainless steel test section tube. The electrical heater is then secured to the outer surface of the copper block. The high conductivity of the copper relative to the stainless steel will ensure a nearly uniform temperature at the wall of the stainless tube. The copper block is joined to the stainless steel test section tube using a silver brazing operation. There is no effective non-destructive test that is readily available in order to verify the continuity of the joint

material in the annulus between the copper block and the stainless tube. In order to reduce the possibility of voids within the joint material, silver braze is applied to one end of the copper block/stainless tube assembly until the braze melt appears around the entire circumference of the joint at the opposite end of the assembly. It is still possible that pockets of air are trapped in the braze joint; voids within the joint material will skew the thermal profile at the surface of the test section tube wall. The affect voids have on the thermal profile at the tube wall is likely dependent on the size and location of the voids; the model illustrated in Figure 2.6 assumes that the joint material is continuous and the effect of voids is not taken into consideration.

The temperature of the copper block and test section tube must reach the melt temperature of the silver braze in order for the brazing process to be successful. At these elevated temperatures an oxide layer would quickly form on the inner surface of the test section tube if it were exposed to an oxidizing agent such as air. This is undesirable as it is not clear what affect an oxide layer would have on the thermal-fluid behavior of the test fluid. Therefore, during the brazing process the inner surface of the test section tube is shielded from oxide formation using an inert gas flow.

2.1.5.2 Tube wall temperature measurement

The relatively high conductivity of the copper block leads to the assumption that the copper block is at a uniform temperature. Based on this assumption, the temperature of the block can be measured at any location. The temperature of the copper block is measured by placing two PRTs in holes that are drilled parallel to the test section tube axis in the face of the copper block. To ensure good thermal contact with the copper

block, the PRT holes are filled with conductive grease prior to PRT insertion. A detailed drawing of the test section copper block is shown in Fig. 2.4 and a photograph is shown in Fig. 2.5.

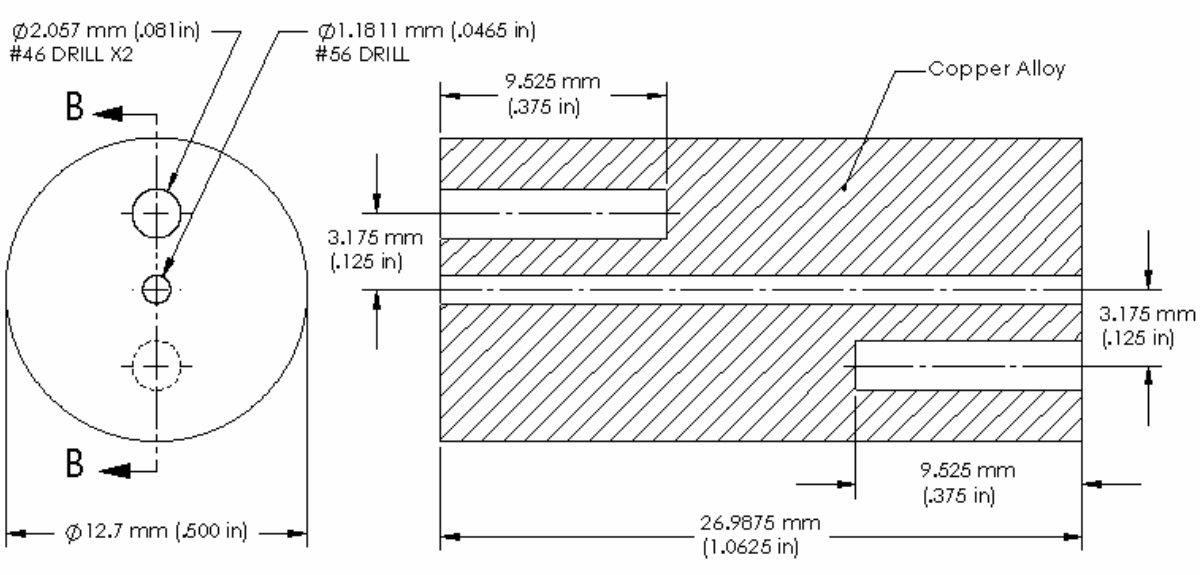

Figure 2.4. Technical Drawing of the test section copper block

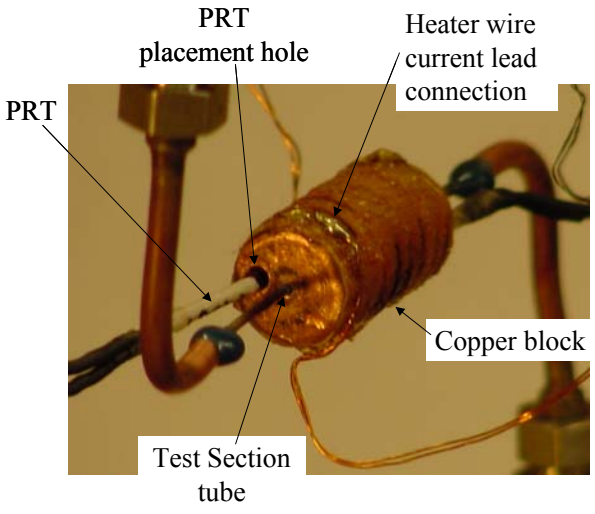

Figure 2.5. Placement of PRT temperature sensors in copper block

The temperature of the inner surface of the test section tube is the temperature of the copper block less the temperature gradient across the copper block and the test section tube wall. The temperature drop in the copper block from the PRT insertion hole to the

outer surface of the test section tube, a radial distance of 2.64mm (0.104in) is estimated using a thermal resistance analysis:

$$\Delta T_{block} = \dot{q}_{applied} R_{block} \tag{2.16}$$

where:

$$R_{block} = \frac{\ln\left(\frac{D_{PRT}/2}{D_o/2}\right)}{2\pi k_{cu} L} \tag{2.17}$$

where k_{cu} is the thermal conductivity of copper. The nominal temperature drop across in the copper block is 0.21 K at 90 K and a heat load of 10 W. The temperature drop across the 0.127mm [0.005in] thick tube wall is estimated using a thermal resistance analysis:

$$\Delta T_{wall} = \dot{q}_{applied} R_{wall} \tag{2.18}$$

where:

$$R_{wall} = \frac{\ln\left(\frac{D_o/2}{D_i/2}\right)}{2\pi k_{ss} L} \tag{2.19}$$

where k_{ss} is the thermal conductivity of stainless steel. The nominal temperature drop across the tube wall is 1.80 K at 90 K and a heat load of 10 W.

2.1.5.3 Measurement of Heat Load Applied to Fluid

The power supplied to the electrical heater ($\dot{q}_{heater}$) is determined by multiplying the applied voltage with the measured current.

$$\dot{q}_{heater} = V I \tag{2.20}$$

The current is measured using an HP 34401A multimeter that is placed in series with the power supply and the resistive element. The voltage drop across the heater is measured with an HP 34401A multimeter; voltage taps are connected at the solder joint between the current leads and heater wire. The heat applied to the fluid stream is equal to the heat applied by the electrical heater less some fraction of heat lost to the surroundings, according to Eq. 2.21.

$$\dot{q}_{heater} = \dot{q}_{applied} + \dot{q}_{loss} \tag{2.21}$$

To determine the heat load applied to the fluid stream, the heat transfer between the test section and its surroundings must be quantified. Figure 2.6 describes the various thermal paths that are available for the heat applied by the electrical heater.

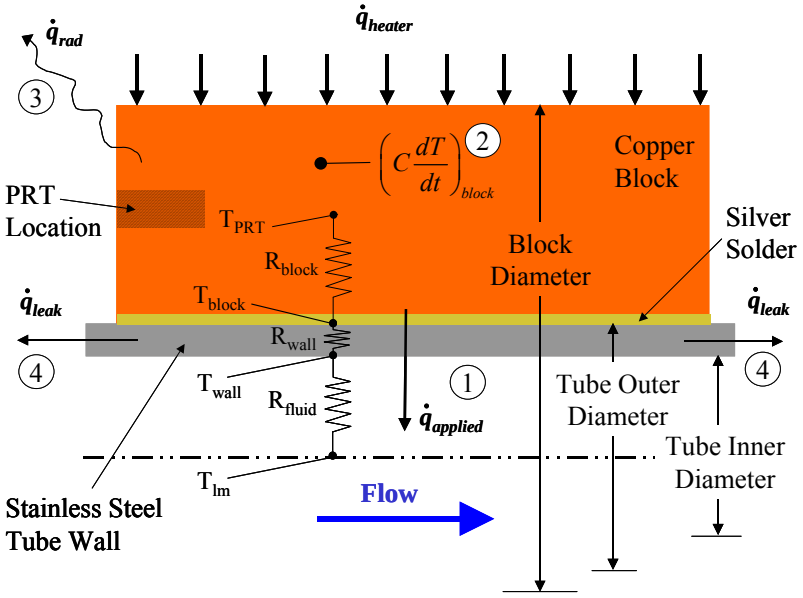

Figure 2.6. Thermal paths available to the heat applied by the electrical heater

The heat applied to the test section can be transferred by convection to the fluid flowing through the test section tube (this is the desired path and is labeled as path 1 in Fig. 2.6). The heat applied to the test section may also be stored by the thermal capacitance of the

copper block (path 2), radiated to the surrounding components and vacuum vessel walls (path 3), or conducted to the adjacent structure (path 4).

At steady state, the thermal capacitance of the copper block does not affect the heat load applied by the electrical heater. However, the thermal mass of the copper block is the primary factor that determines the time that is required for the test section to reach an acceptable steady state. The capacitance of the copper block (C_{block}) is determined from its volume (V_{block}) together with the density (ρ_{Cu}) and specific heat capacity (c_{Cu}) of copper.

$$C_{block} = \rho_{Cu} V_{block} c_{Cu} \tag{2.22}$$

The thermal capacitance of the copper block at room temperature is nominally 11.31 J/K. The copper block communicates thermally primarily with the fluid. If the fluid conditions are approximately constant, Eq. 2.22 defines the time constant (τ_{block}) required for the test section to approach steady state. At room temperature, the copper block has a time constant of nominally 30 sec with a heat transfer coefficient of 5000 W/m^{2}K and 8 sec with a heat transfer coefficient of 20,000 W/m^{2}K.

$$\tau_{block} = \frac{C_{block}}{htc\, A_s} \tag{2.23}$$

The test section is placed in a vacuum vessel which is evacuated using a turbomolecular pump to a pressure of less than 1x10^{-3} torr. At this pressure convective heat transfer is essentially eliminated. Three layers of radiation shielding, consisting of alternating layers of Dacron netting and aluminized Mylar, are used to insulate the test section from

radiation heat transfer. The radiation heat transfer is calculated based on the geometry of the test section, multiple radiation shields and a 0.05 shield emissivity. The radiation heat leak is 15.5 mW for a test section temperature of 90 K and a vessel wall temperature of 293 K. This is a negligible heat transfer rate relative to the applied load.

Conductive heat transfer dominates the fraction of the applied heat that is lost to, or gained from, the surroundings. In order to determine the amount of conductive heat transfer for each measurement of applied heat load, it is necessary to characterize the thermal resistance between the test section and the surrounding structure. The thermal resistance that characterizes this conduction heat leak has been determined experimentally. The experiment was operated at room temperature in a condition where both the vacuum vessel and the internal fluid passages are evacuated. A small (15 mW) heat load is applied to the test section in order to generate a temperature difference between the surrounding structure and the test section. The temperature of the surrounding structure is characterized by the temperature measured at the temperature measurement headers that are used to measure the fluid inlet and exit temperatures. The temperature of the test section and the two temperature measurement headers as a function of time is illustrated in Fig. 2.7. Notice that the 14.5 mW heat load results in nominally an 8.0 K temperature difference between the block and the surrounding structure.

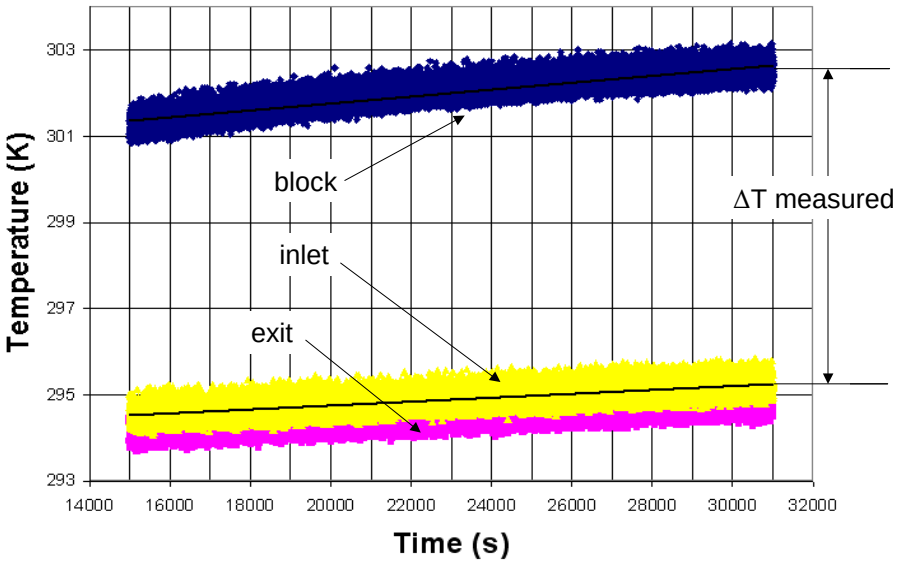

Figure 2.7. Temperature of the block and temperature measurement headers as a function of time with a 14.5 mW heat load applied and the test facility evacauted (both the vacuum space and fluid passages). The ratio of the temperature difference and applied heat load is associated with the conductive resistance between the test section and the adjacent structure.

The temperature difference together with the heat load applied during the "no-flow" test is used to calculate the thermal resistance associated with the conduction heat leak (R_{leak}).

$$R_{leak} = \frac{T_b - \frac{T_1 + T_2}{2}}{\dot{q}_{applied}} \tag{2.24}$$

The resulting thermal resistance of the conduction heat leak is 550 K/W. At an inlet temperature of 90 K and a 10 W heat load, the resulting heat leak represents an error of nominally 0.30%. During the analysis of experimental data, the heat transfer applied to the heater is adjusted using the resistance value measured above in order to estimate the actual heat load applied to the fluid.

2.1.5.4 Fluid Temperature Measurement

Accurate measurement of the heat transfer coefficient requires accurate measurement of the fluid temperature at the inlet and exit to the test section and the temperature of the test section tube wall. The predictable nature of conduction heat transfer within the block makes the measurement of the tube wall reliable. The PRTs used to measure the fluid temperature are submerged in the fluid and therefore the fluid temperature is communicated to the PRT by convection. An accurate measure of the fluid stream temperature requires a low thermal resistance between the PRT and fluid stream as well as a high thermal resistance between the PRT and the supporting structure and the electrical pass-thru used to carry the temperature signal out of the hermetic fluid passages. The temperature measurement headers were designed to meet these criteria. The thermal path of least resistance to the platinum sensor element is through the PRT leads and therefore it is important that the leads are thermally staked to the fluid. The current supply and voltage measurement wires are connected to the PRT leads so that the leads protrude from the PRT body on the end of the sensor that is opposite to the pass-thru. The leads can therefore be exposed to the fluid passing over the sensor before they reverse direction where they are attached to the 4-wire terminals that pass through the tube wall. This configuration is shown schematically in Fig. 2.8. A photograph of the PRT is shown in Fig. 2.9.

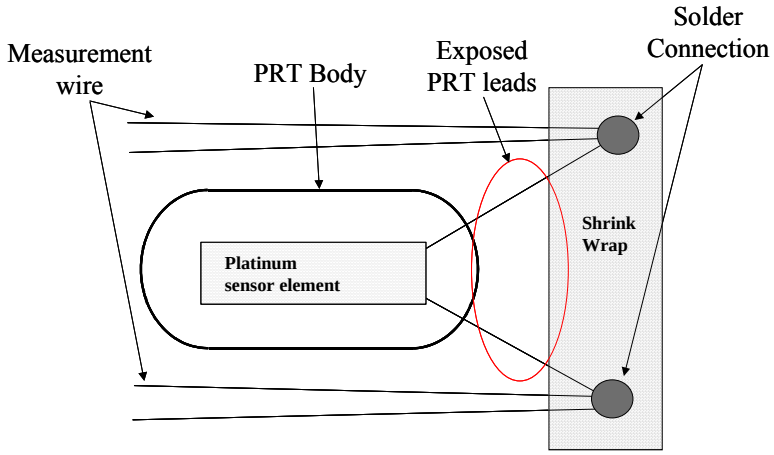

Figure 2.8. Schematic of PRT lead orientation

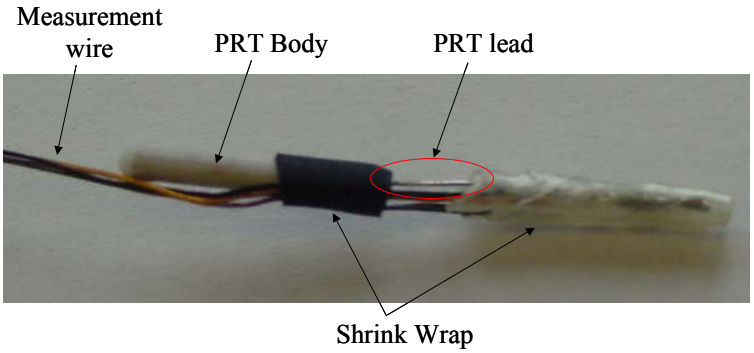

Figure 2.9. Picture of PRT lead orientation

To isolate the PRT from the surrounding tubing, a G-10 composite and stainless steel safety wire is used to suspend the PRT in the center of the tube, as illustrated in Fig. 2.10. The safety wire provides mechanical support to the PRT, reducing the possibility of damage to the PRT body or leads and ensuring that the PRT is not touching the tube wall. The G-10 provides thermal isolation between the PRT and the hermetic pass through. The PRT measurement wires are tightly wrapped around both the PRT body and the steel safety wire in order to secure the PRT.

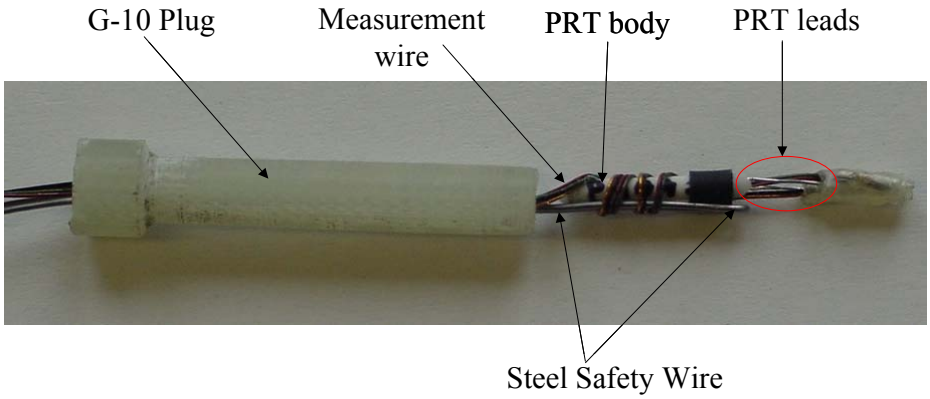

Figure 2.10. Fluid penetration PRT assembly component

The PRT and G-10 plug assembly are then placed in a tube stub which is inserted into one end of a copper tee, as shown in Figures 2.11 and 2.12. The tee and tube are soldered together with tin-lead soft solder prior to the insertion of the PRT/G-10 assembly. Each temperature measurement header contains two of these assemblies. Once all of the associated tubing is soldered together, the PRT/G-10 assembly is epoxied into the tube stub using Stycast 2850. The epoxy joint is done last in order to avoid burning the epoxy or thermally damaging the PRT during the solder operations.

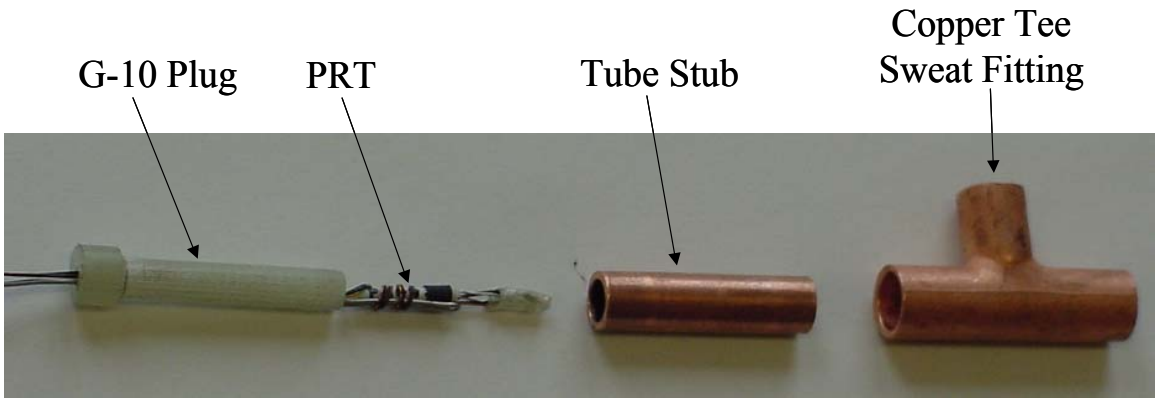

Figure 2.11. Break-out view of the temperature header

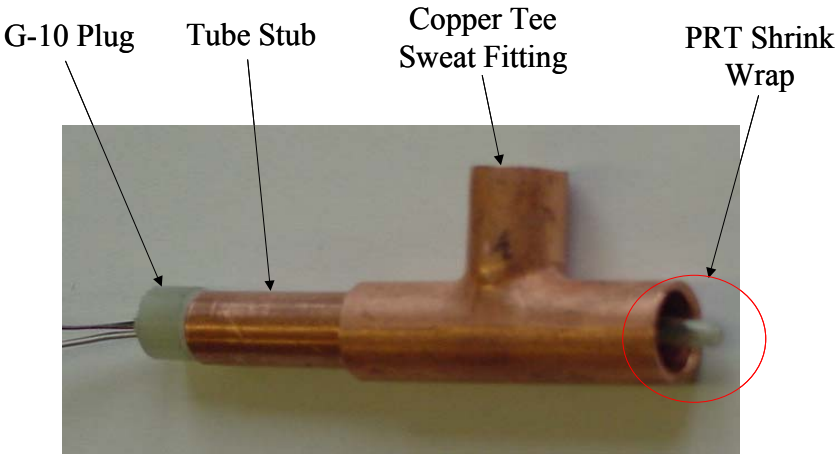

Figure 2.12. Assembled temperature measurement header

2.1.6 Test Section Fabrication

The test facility, shown as an exploded view in Figure 2.13, is constructed primarily of commercial copper refrigeration tubing and 60/40 Tin/Lead solder for each tube joint. Stainless steel tubing, silver braze, and Stycast 2850 epoxy are used in a few specific locations, such as the pressure taps, stainless steel VCR fittings and the joining of copper and stainless steel components. The test facility is designed to carry out the measurement objectives, fit within the space restraints of the vacuum space, and provide a modular test section assembly. Modularity is achieved by connecting the test section assembly to the temperature measurement headers with VCR fittings. VCR fittings use a metal gasket compressed between two stainless steel bodies resulting in a highly reliable seal. A modular test section enables the primary objective of providing local heat transfer coefficient data relevant to the numerical model of a recuperative heat exchanger.

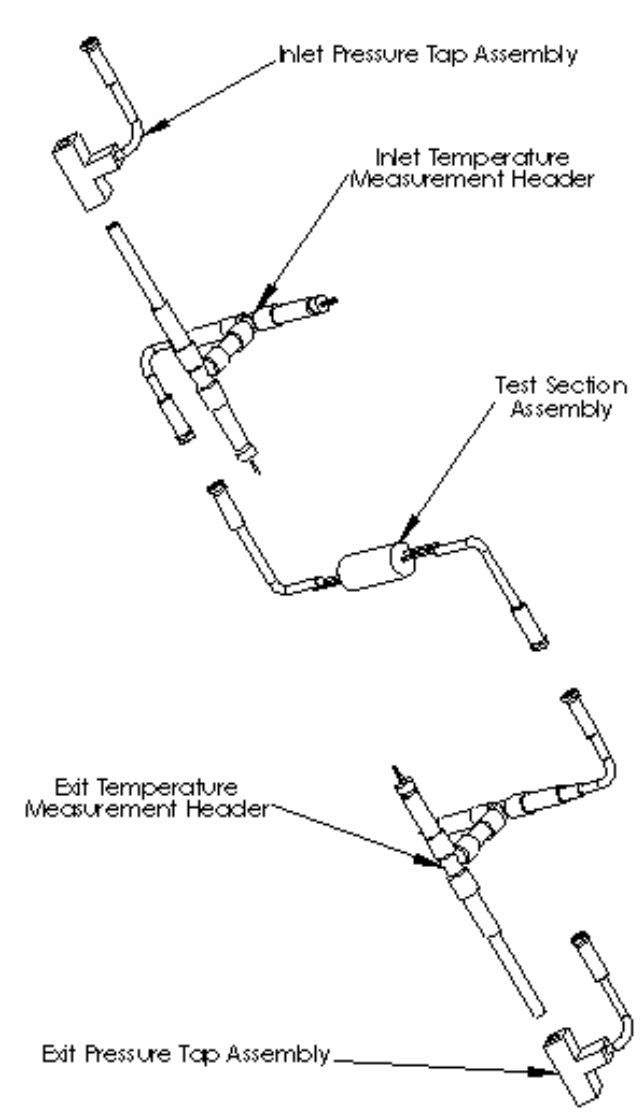

Figure 2.13. Exploded view of the Test Section

2.1.6.1 Pressure Tap Assembly

The pressure tap assembly is composed of three elements: a copper sweat tee, VCR fitting, and a short length of stainless steel tubing as shown in Figure 2.14. The lack of a commercially available copper sweat tee of the desired tube size required the fabrication of the part depicted. Silver braze is used to join the VCR fitting to the stainless steel tube, and the stainless steel tube to the copper sweat tee. The silver braze is chosen for ease of use with stainless steel and stainless steel to copper joints.

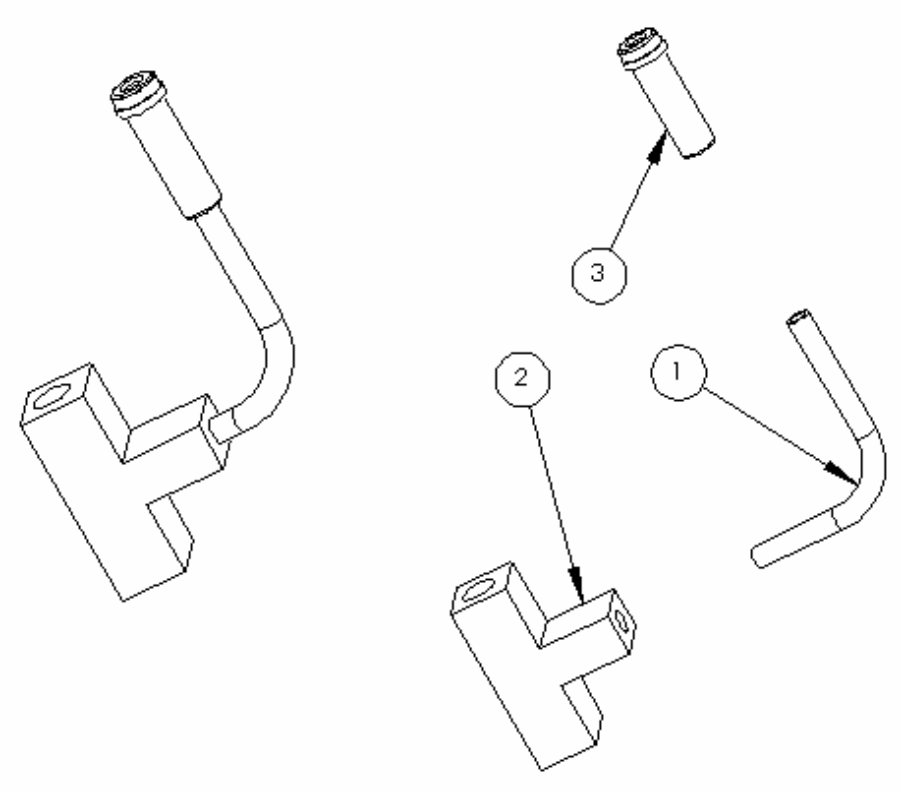

Item No.	Description
1	∅3.175mm, 0.762mm wall SS 304 Tubing (∅0.125in, 0.030in wall)
2	∅4.763mm to ∅3.175mm Copper Sweat Tee (∅0.1875in to ∅0.125in)
3	SS-2-VCR-3 Copper Gasket Fitting

Figure 2.14. Exploded view of the Pressure Tap Assembly

Figure 2.15. The Pressure Tap Assembly integrated into the Test Facility

2.1.6.2 Temperature Measurement Header

As described earlier, the temperature measurement header has the task of placing the PRT in the center of the bulk fluid stream, thermally isolating the PRT element, and ensuring that enough mixing occur that the PRT element is in thermal contact with the bulk fluid temperature. Figure 2.16 shows an exploded view of the inlet temperature measurement header. In addition to the requirements stated, the temperature measurement header must fit inside the vacuum space, and integrate smoothly with surrounding test section components. Copper tees were used to conserve space, and provide a penetration point for the PRT probe assemblies.

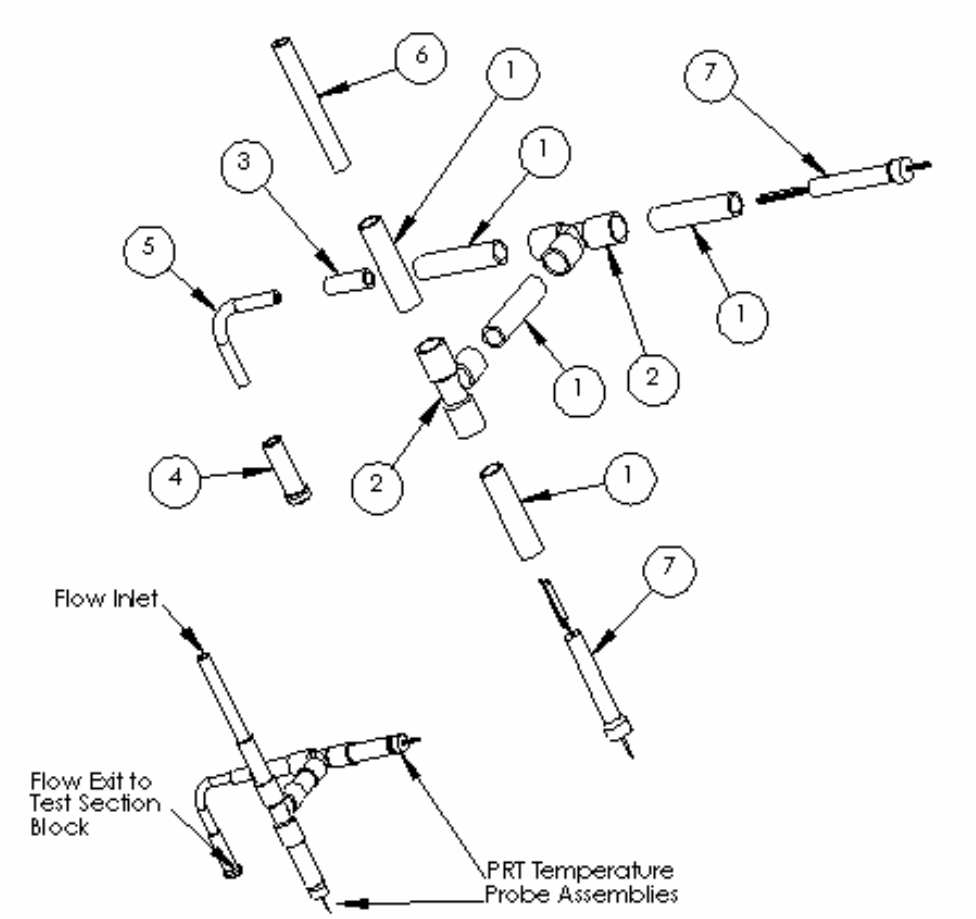

Item No.	Description
1	∅6.35 mm (0.250 in), 0.762mm (0.030 in) wall Copper Refrigeration Tubing
2	∅6.35 mm (0.250 in) Copper Sweat Tee
3	∅4.763 mm (0.1875 in), 0.762 mm (0.030 in) wall Copper Refrigeration Tubing
4	SS-2-VCR-3 Copper Gasket Fitting
5	∅3.175 mm (0.125 in), 0.762 mm (0.030 in) wall Copper Refrigeration Tubing
6	∅4.763 mm (0.1875 in), 0.762 mm (0.030 in) wall Copper Refrigeration Tubing
7	PRT Temperature Probe Assembly

Figure 2.16. Exploded view of Temperature Measurement Header

The PRT probe assembly, Figure 2.17, is comprised of three main components: a G-10 plug, stainless steel safety wire, and the PRT element.

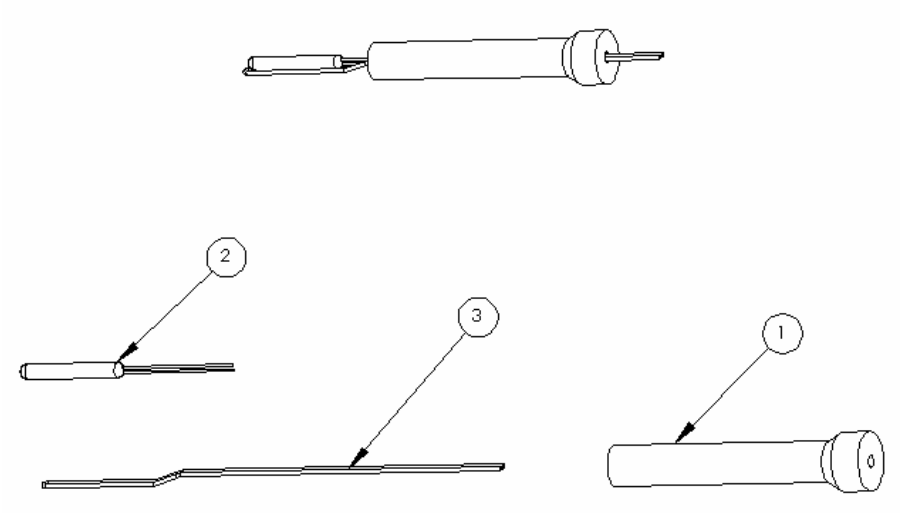

Item No.	Description
1	G-10 composite plug
2	Lakeshore PT-103 Platinum Resistive Thermometer
3	∅ 0.508 mm (0.020 in) SS316 safety wire

Figure 2.17. Exploded view of the PRT probe assembly

The G-10 plug is machined to fit the inner diameter of the intended tubing plus a minimal amount of clearance, Figure 2.18. The length of the G-10 plug is determined so that the PRT element emerging from the end is in the path of the flow entering (or exiting) the copper tee.

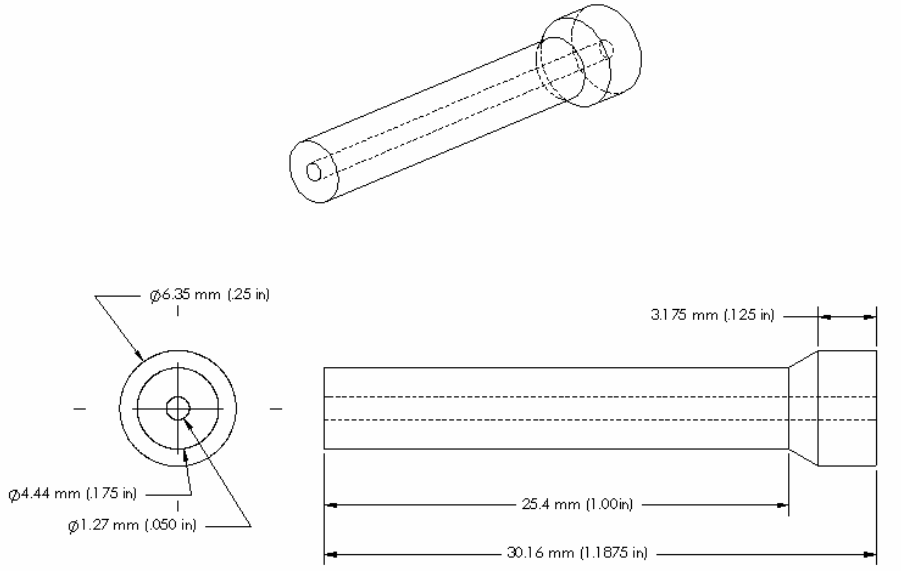

Figure 2.18. Drawing of the G-10 plug

2.1.6.3 Test Section Assembly

The test section assembly is constructed by silver brazing two short sections of copper tubing each to a VCR fitting, silver brazing a small stainless steel tube to a copper block, and epoxying the end of the copper tubes opposite the VCR fittings to each end of the stainless steel tube as shown in Figure 2.19.

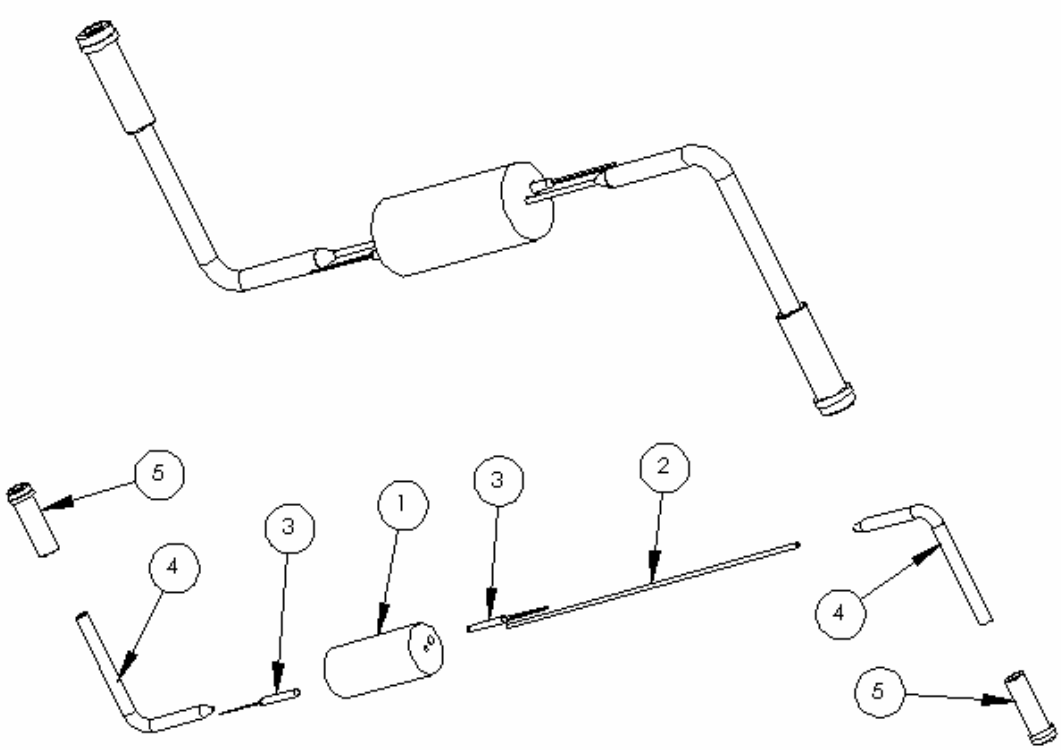

Item No.	Description
1	∅12.7mm (0.500 in), 26.988mm (1.0625 in) length 110 Copper Alloy Test Section Block
2	∅1.067mm (0.042in), 0.127mm (0.005in) wall SS 304 Tubing
3	Lakeshore PT-103 Platinum Resistive Thermometer
4	∅3.175mm (.125 in), 0.762mm (.03 in) wall Copper Refrigeration Tubing
5	SS-2-VCR-3 Copper Gasket Fitting

Figure 2.19. Exploded view of Test Section Assembly

2.2 Mechanical Design

The test fluid must be pre-conditioned to achieve the specific test conditions that are required to complete the experimental objectives set out in the preceding section. Table 2.2. lists the test condition requirements.

Table 2.2. Test Condition Requirements

Minimum Inlet Temperature	90 K
High Inlet Pressure	1500 kPa
Low Inlet Pressure	100 kPa
Mass Flow Rate	0.6 g/s

The pre-conditioning of the fluid is accomplished using a combination of a GM Cryocooler and a recuperative heat exchanger.

2.2.1 GM Cryocooler

A Cryomech AL60 cryocooler, pictured in Figure 2.20, is used to provide the cooling that is required to reduce the temperature of the fluid to the test condition inlet temperature.

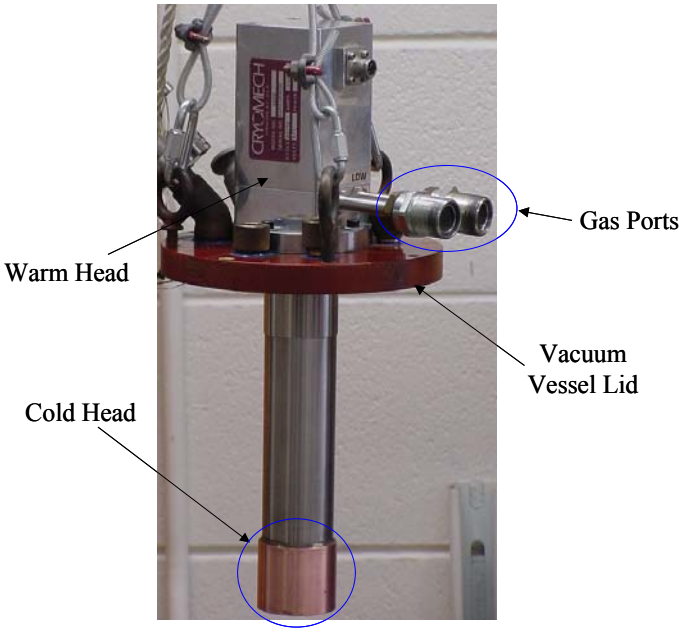

Figure 2.20. Cryomech AL60, GM type cryocooler

The AL60 cryocooler (Cryomech, 2004) is a commercially available, Gifford-McMahon type cryocooler. The manufacturer specifies the cooling capacity of the cryocooler to be 60 W at 80 K. The test fluid communicates thermally with the cryocooler via the cryocooler heat exchanger that is bolted to the cold head.

2.2.2 Cryocooler Heat Exchanger Design

The general form of the cryocooler heat exchanger is a cylindrical copper block with an outer diameter of 50.8 mm (2.0 in) in order to match the diameter of the cryocooler cold head, D_c. Helically wound, commercially available refrigeration tubing with an outer diameter, $D_{o,tube}$, of 4.77 mm (0.188 in) is mechanically and thermally fastened to the cylindrical block using lead/tin soft solder, as shown in Figure 2.21. The cryocooler heat exchanger bolts to the cryocooler through counter-bored holes that are drilled in the copper block.

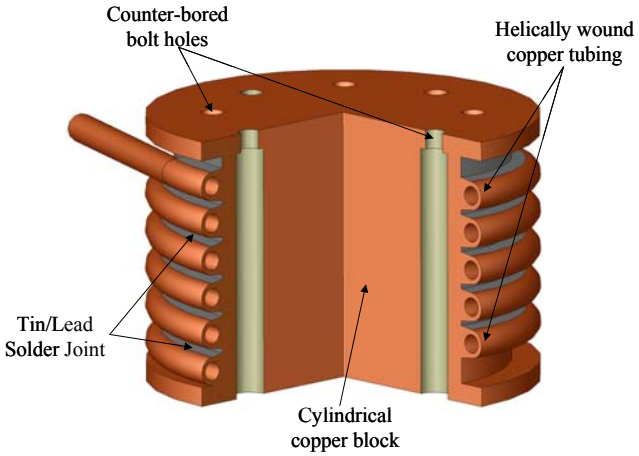

Figure 2.21. Solid model of the cryocooler heat exchanger

An indium gasket is placed between the cryocooler heat exchanger and the cryocooler in order to reduce the thermal contact resistance. The cryocooler heat exchanger is shown attached to the cryocooler in Figure 2.22.

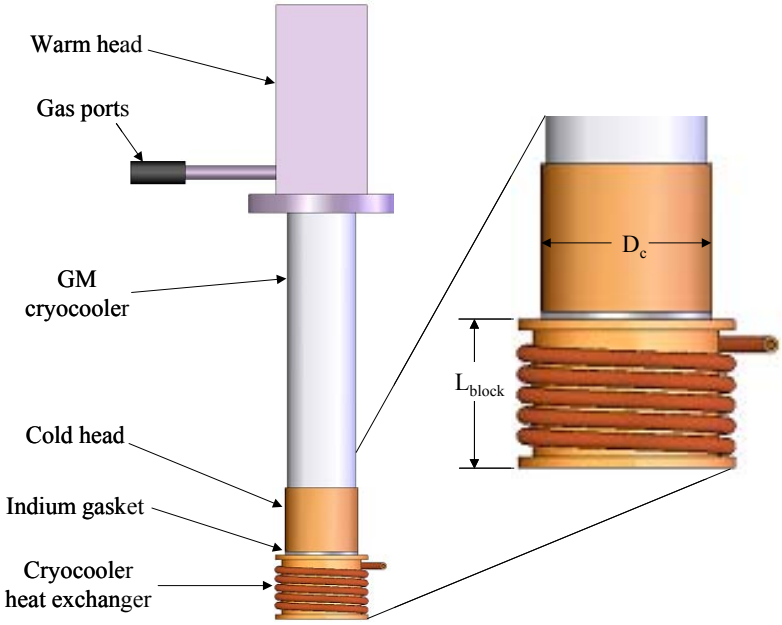

Figure 2.22. GM cryocooler and heat exchanger assembly

The length of the heat exchanger tubing and heat exchanger block, L_{block}, is determined from a thermal analysis that balances the increased heat exchanger effectiveness associated with a longer block with the increased conduction resistance that results from a longer thermal path.

The heat exchanger analysis is based on a simple one-dimensional resistor network, as shown in Figure 2.23. Three resistors make up the network: the convection resistance, R_{conv}, from the fluid to the tube wall; the conduction resistance, R_{cond}, of the interfaces of the tube and the copper block and the copper block and the cryocooler; and the contact resistance, R_{cont}, across the indium gasket that separates the cryocooler heat exchanger from the cryocooler. The total conductance, UA, which separates the fluid passing through the cryocooler heat exchanger and the cryocooler cold tip is calculated based on this resistor network.

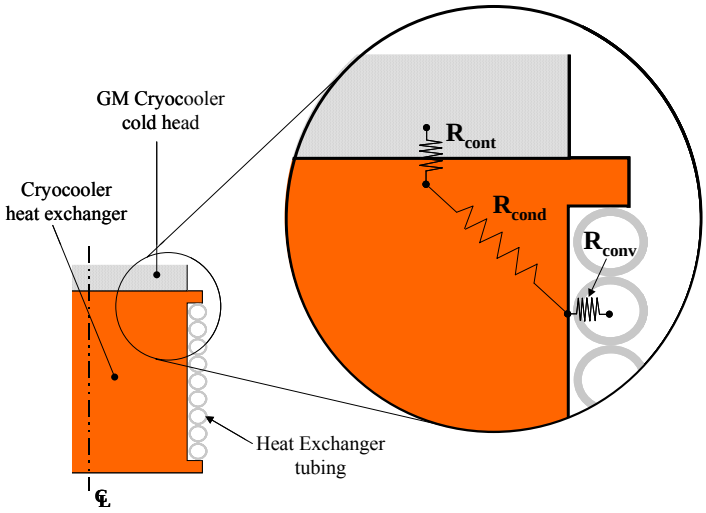

Figure 2.23. Cross-sectional view of cryocooler heat exchanger depicting the one-dimensional resistor network

To conservatively estimate the performance of the heat exchanger, we assume laminar (as opposed to turbulent) flow of nitrogen vapor inside the heat exchanger tubing. The convection resistor is defined as:

$$R_{conv} = \frac{1}{htc\, A_s} \tag{2.25}$$

where:

$$A_s = \pi D_{i,tube} L_{tube} \tag{2.26}$$

and

$$L_{tube} = \pi (D_c + D_{o,tube}) N_T \tag{2.27}$$

where *htc* and N_T are the heat transfer coefficient of the fluid and the number of turns of tubing, respectively. The Nusselt number for laminar flow is a constant 4.36 at a mass flow rate of 1 g/s.

The temperature drop across the wall of the tubing is neglected, and a uniformly applied heat load at the block surface is assumed. Figure 2.24 describes the two-dimensional conduction of heat from the cylindrical surface of the heat exchanger block to the cold head of the GM cryocooler.

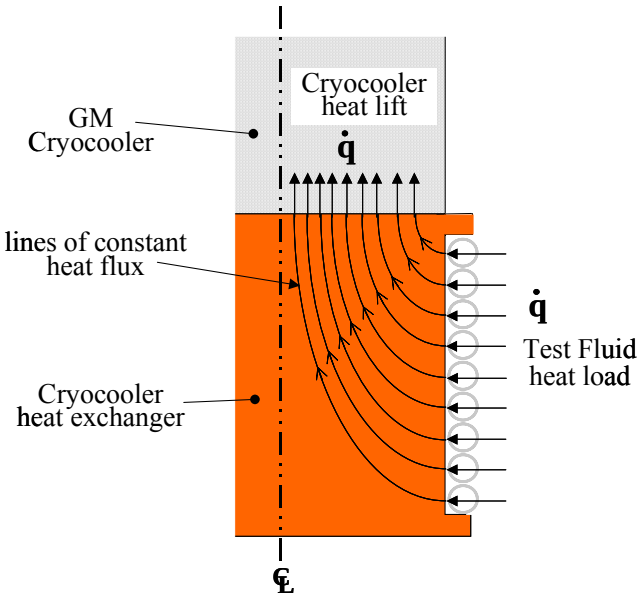

Figure 2.24. Schematic representation of heat flow within the copper block of the cryocooler heat exchanger

In order to simplify the 2D conduction heat transfer problem shown in Fig 2.24 to a one-dimensional thermal resistor, a conduction length and area is assumed. The conduction resistor is calculated as a one-dimensional plane wall thermal resistance:

$$R_{cond} = \frac{L_{cond}}{k_{Cu} A_{cond}} \tag{2.28}$$

where:

$$L_{cond} = \frac{3}{8}\pi L_{block} \tag{2.29}$$

and

$$A_{cond} = \frac{1}{4}\pi D_c^2 \tag{2.30}$$

$$L_{block} = D_c \left(\#turns \right) \tag{2.31}$$

The contact resistance, R_{cont}, for an Indium gasket at a contact pressure of 100 kN/m^2 (14.5psi) is 0.0001421 K/W (Incropera, 2002).

The heat exchanger effectiveness is determined based on the number of transfer units (*NTU*) of the heat exchanger.

$$NTU = \frac{UA}{\dot{m}\, c_P} \tag{2.32}$$

where:

$$UA = \frac{1}{\sum R} = \frac{1}{R_{cont} + R_{cond} + R_{conv}} \tag{2.33}$$

where c_P is the constant pressure specific heat capacity of the fluid being tested. Equation 2.34 presents the relationship for effectiveness (ε) as a function of *NTU* for a heat exchanger with a capacitance ratio equal to zero (Incropera, 2002).

$$\varepsilon = 1 - e^{-NTU} \tag{2.34}$$

Figure 2.25 is a plot of the NTU and effectiveness of the cryocooler as a function of the number of turns of tube.

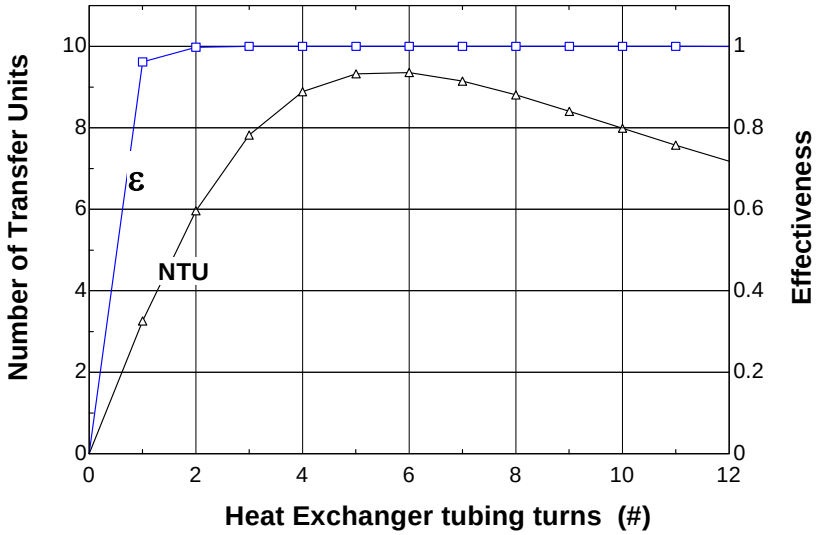

Figure 2.25. Heat Exchanger NTU and Effectiveness as a function of number of tubing turns

While an optimum heat exchanger configuration exist at approximately 6 turns, the effectiveness of the heat exchanger is effectively one for turns greater than 2. The cryocooler heat exchanger is constructed with 8 turns, as shown in Figure 2.26.

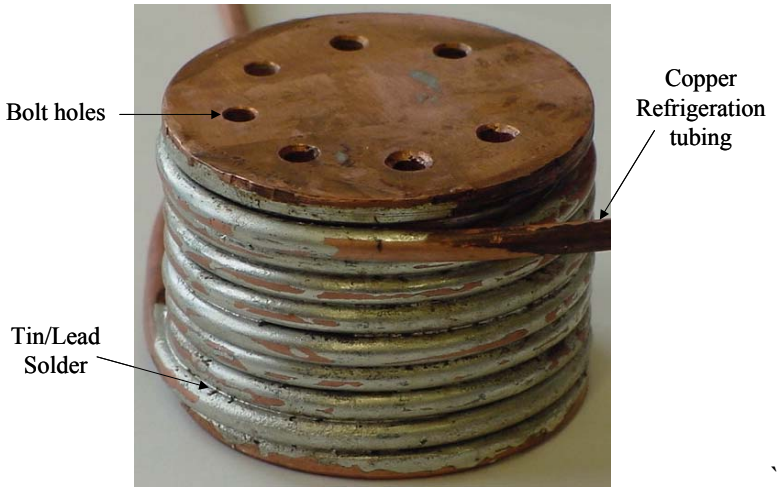

Figure 2.26. Photograph of completed cryocooler heat exchanger

Figure 2.27. presents the final dimensions of the cryocooler heat exchanger.

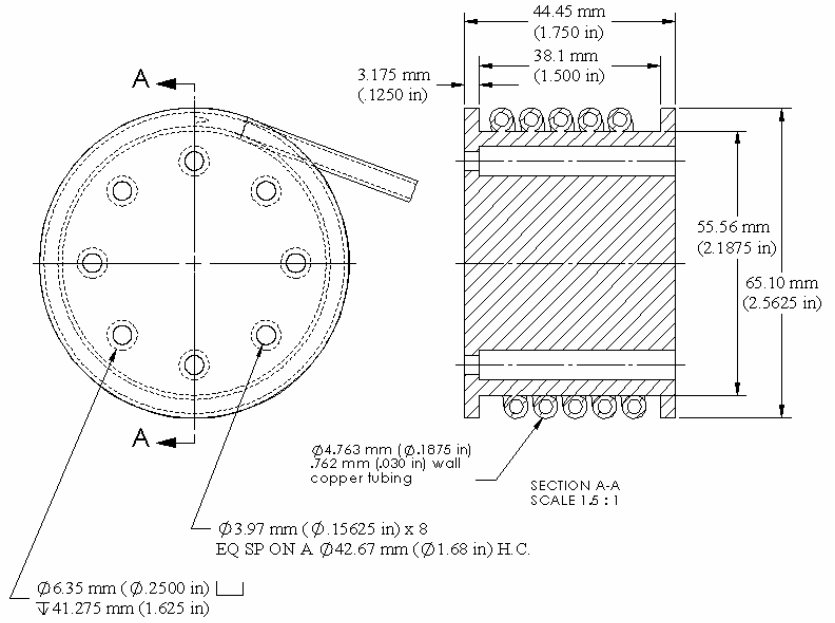

Figure 2.27. Detailed drawing of the cryocooler heat exchanger

To determine the approach temperature required for an exit temperature of 90 K, the cooling power of the cryocooler at 80 K is set equal to the heat exchanger effectiveness, multiplied by the change in energy of the fluid across the heat exchanger; Eq 2.35.

$$\dot{q}_{AL60} = \varepsilon \dot{m} c_P \left(T_{approach} - T_{exit} \right) \tag{2.35}$$

where $T_{approach}$ and T_{exit} are the fluid approach temperature and exit temperature, respectively. Eq 2.35. assumes the fluid specific heat capacity does not change significantly over the temperature range. The resulting maximum allowable approach temperature for an exit temperature of 90 K is 130 K based on the cryocooler load capability. Because the cryocooler is not capable of cooling the fluid from room temperature to the test conditions, a recuperative heat exchanger is required in order to reduce the temperature of the incoming fluid to the maximum allowable approach temperature of the cryocooler heat exchanger.

2.2.3 Recuperative Heat Exchanger Design

The required effectiveness of the recuperative heat exchanger used to pre-cool the test fluid before it enters the cryocooler heat exchanger is determined from the approach temperature calculated using Eq. 2.35. Heat exchanger effectiveness is defined as the ratio of the actual heat transfer rate ($\dot{q}_{HX}$) for a heat exchanger to the maximum possible heat transfer rate ($\dot{q}_{\max}$) (Incropera, 2002); Eq 2.36.

$$\varepsilon \equiv \frac{\dot{q}_{HX}}{\dot{q}_{\max}} \tag{2.36}$$

The minimum required heat exchanger effectiveness is determined by setting the maximum heat transfer rate equal to the change in energy of the fluid from the exit of the test section to room temperature:

$$\dot{q}_{\max} = \dot{m}\left[h\left(300\text{ K}, P\right) - h\left(90\text{ K}, P\right)\right] \tag{2.37}$$

where h is the enthalpy of the fluid. The actual heat transfer rate of the recuperative heat exchanger is equal to the change in enthalpy required to reduce the temperature of the fluid to the required approach temperature for the cryocooler heat exchanger (130 K).

$$\dot{q}_{\max,HX} = \dot{m}\left[h\left(300\text{ K}, P\right) - h\left(130\text{ K}, P\right)\right] \tag{2.38}$$

The resulting minimum required heat exchanger effectiveness is found to be 0.80.

The vacuum vessel in which the test facility is placed has an inner diameter of 127 mm (5.0 in); the available space within the vacuum vessel is considered when determining the general dimensions of the recuperative heat exchanger. A paired tube heat exchanger, wound helically, is chosen as the basic configuration for the heat exchanger. Commercial refrigeration tubing with an outer diameter of 3.18 mm (0.125 in) is used for the

recuperative heat exchanger. Figure 2.28. depicts the general shape of the heat exchanger. The diameter of the coil, the nature of the joint between the tubes and the tubing size are all specified by manufacturing requirements. The remaining free parameter is the heat exchanger length.

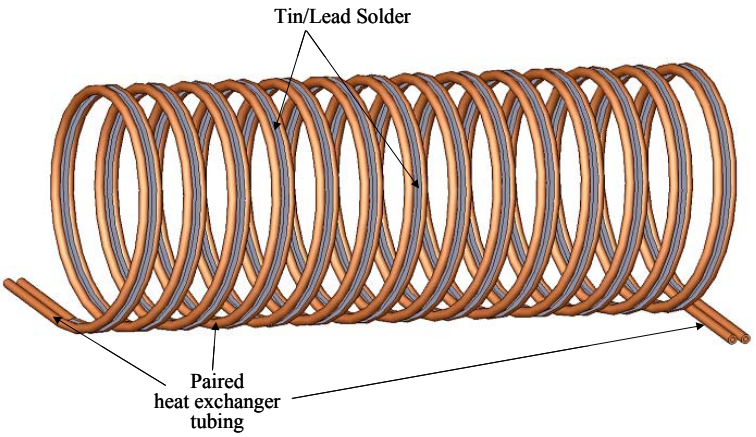

Figure 2.28. Helically wound, paired-tube recuperative heat exchanger configuration

The required heat exchanger length is specified based on the heat exchanger effectiveness.

Figure 2.29. shows a cross-sectional view of the heat exchanger with a superimposed one-dimensional thermal resistor network and a lead/tin solder joint between the tubes. The one-dimensional resistor network shown in Fig. 2.29 is used to determine the *NTU* and effectiveness of the recuperative heat exchanger.

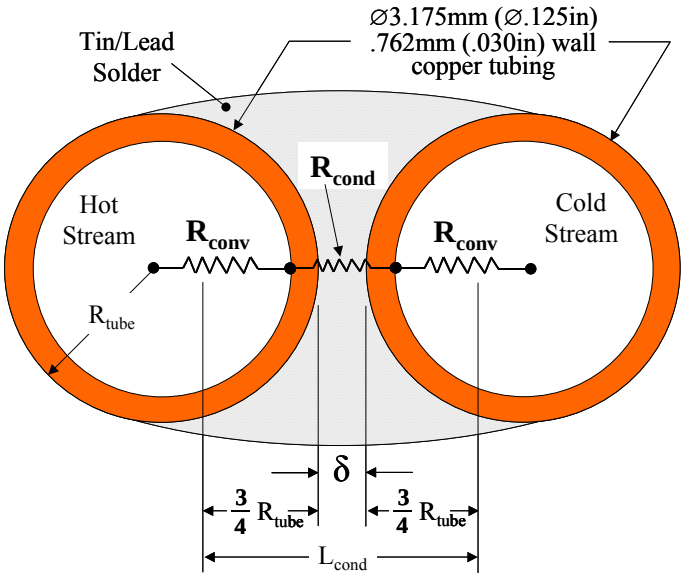

Figure 2.29. Cross-sectional view of recuperative heat exchanger

The convective thermal resistances represent the heat transfer from each fluid stream to their respective tube wall. Laminar flow of pure nitrogen vapor is used as a conservative estimate of the convection heat transfer.

$$R_{cond} = \frac{1}{htc\, A_s} \tag{2.39}$$

where:

$$htc = \frac{Nu\, k_f}{D_{i,tube}} \tag{2.40}$$

and

$$A_s = \frac{1}{2}\pi D_{i,tube} L_{HX} \tag{2.41}$$

where Nu, k_f, $D_{i,tube}$, and L_{HX} are the Nusselt number of the fluid, the conductivity of the fluid vapor, the tube inner diameter, and the length of the heat exchanger tubing respectively. The fluid is assumed to be laminar, resulting in a constant Nusselt number of 4.36. The convection area is set as half of the inner tube surface area to further ensure

a conservative assumption in the determination of the heat exchanger NTU and effectiveness.

A one-dimensional plane wall conduction resistor defines the conduction heat transfer:

$$R_{cond} = \frac{L_{cond}}{k_{Cu}\, A_{cond}} \tag{2.42}$$

where L_{cond}, A_{cond}, and k_{Cu} are the conduction length, conduction area, and conductivity of copper respectively. The conduction geometry is not a simple plane wall and therefore an appropriate conduction area and length must be determined in order to ensure a conservative estimate of the heat exchanger performance. Figure 2.29. displays the one-dimensional conduction length, L_{cond}, that is chosen to represent the two-dimensional conduction path.

$$L_{cond} = \frac{3}{2} R_{tube} + \delta \tag{2.43}$$

where R_{tube}, and δ are the inner radius of the tube and the distance separating the tubes respectively. The one-dimensional conduction area, A_{cond}, is defined as:

$$A_{cond} = D_{o,tube} L_{HX} \tag{2.44}$$

where $D_{o,tube}$ is the outer diameter of the tube.

Equation 2.45 relates NTU and capacitance ratio, C_r, to the effectiveness of the heat exchanger.

$$\varepsilon = \frac{1 - e^{\left[-NTU(1-C_r)\right]}}{1 - C_r e^{\left[-NTU(1-C_r)\right]}} \tag{2.45}$$

where

$$C_r = \frac{C_{min}}{C_{max}} \tag{2.46}$$

and C_{min} and C_{max} are the minimum and maximum capacity rates of the two streams, evaluated at each stream's respective inlet temperature:

$$C_{\min} = MIN\left(C_{in,hot}, C_{in,cold}\right) \tag{2.47}$$

$$C_{\max} = MAX\left(C_{in,hot}, C_{in,cold}\right) \tag{2.48}$$

where

$$C_{in,hot} = \dot{m}\, c_{P,in,hot} \tag{2.49}$$

$$C_{in,cold} = \dot{m}\, c_{P,in,cold} \tag{2.50}$$

The *NTU* of the heat exchanger is related to the total conductance, *UA*, and the minimum stream capacitance, C_{min}, according to

$$NTU = \frac{UA}{C_{\min}} \tag{2.51}$$

where

$$UA = \frac{1}{2\, R_{conv} + R_{cond}} \tag{2.52}$$

The *NTU* and effectiveness of the recuperative heat exchanger are calculated as a function of heat exchanger length and shown in Figure 2.30. Notice that a total length of nominally 2.75 m is necessary to achieve the required effectiveness.

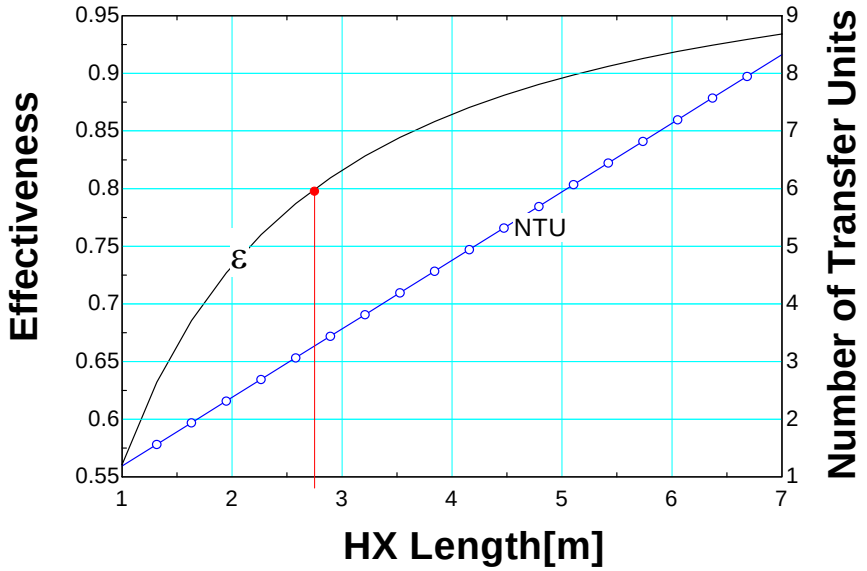

Figure 2.30. Heat Exchanger NTU and Effectiveness as a function of heat exchanger length

Table 2.3. presents the specifications of the recuperative heat exchanger – the actual length is somewhat longer than the 2.75 m requirement. Figure X is a photograph of the completed recuperative heat exchanger prior to integration into the test facility.

Table 2.3. Recuperative Heat Exchanger Specifications

Heat Exchanger Type		Helically Coiled Paired-Tube
Tubing	Type	Commercial Copper Refrigeration Tubing
	Length	3.35 m (132 in)
	Outer Diameter	3.18 mm (.125 in)
	Wall Thickness	.76 mm (.030 in)
Helix Diameter		76.2 mm (3.0 in)
Helix Height		240 mm (9.45 in)
Solder Type		Tin/Lead alloy

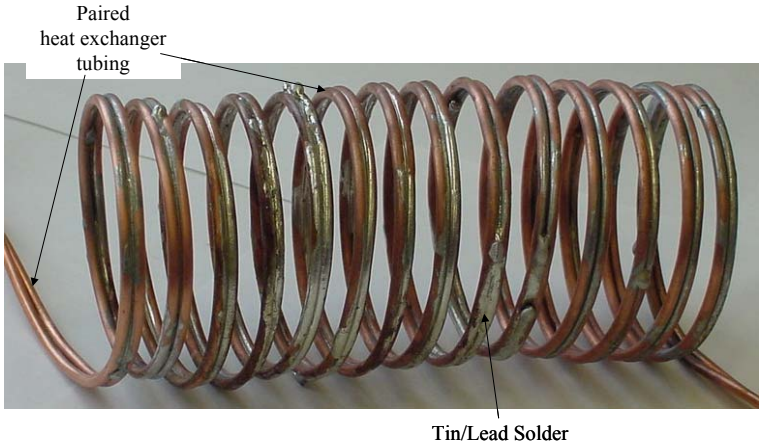

Figure 2.31. Recuperative Heat Exchanger

2.2.4 Test Facility Control

A schematic of the test facility, Figure 2.32., shows the GM cryocooler, cryocooler heat exchanger, recuperative heat exchanger, test section, single-stage compressor, and gas chromatograph interfaced with one another. The key components of the facility are listed in Table 2.4.

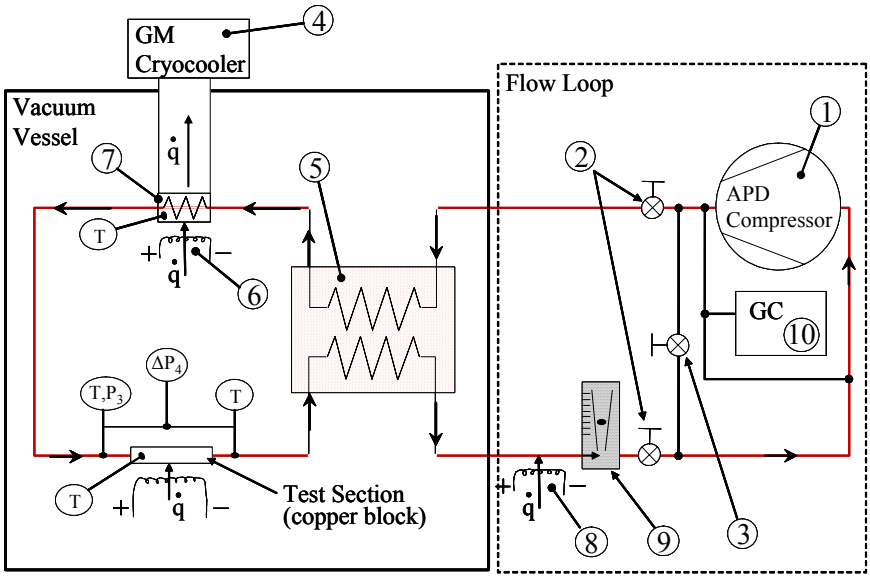

Figure 2.32. Test Facility Schematic

Table 2.4. Test Facility Schematic Key

#	**Component Description**
1	APD HC-2 Compressor
2	Experiment Supply Throttle Valve
3	Bypass Throttle Valve
4	Cryomech AL60 GM Cryocooler
5	Recuperative Heat Exchanger
6	Cryocooler Trim Heater
7	Cryocooler Heat Exchanger
8	Tape Heater
9	Variable Area Flow Meter (Rotameter)
10	Gas Chromatograph

A trim heater (#6 in Figure 2.32.) placed around the circumference of the cold head of the cryocooler controls the inlet temperature to the test section by modulating the cryocooler load. A variable voltage ac transformer provides electrical power to the trim heater. The temperature of the fluid exiting the vacuum vessel is occasionally low enough to be two-phase and therefore not compatible with mass flow measurement devices. A tape heater (#8 in Figure 2.32.) wrapped around the exiting flow tubing heats the fluid to room temperature in order to achieve a single-phase vapor state prior to entering the mass flow meter. The temperature of the fluid, monitored by two redundant fluid stream penetration thermocouples on the low pressure side of the flow loop, is used to determine the power required by the tape heater.

The gas control portion of the test facility is a general facility capable of providing controlled and steady flow of a test fluid to an arbitrary experiment. In addition to the APD HC-2 compressor used to energize the flow, the flow loop is comprised of a gas chromatograph, test fluid construction manifold, and various fluid instrumentation. Figure 2.33. is a schematic of the flow loop and Table 2.5 provides the key to the indicated components.

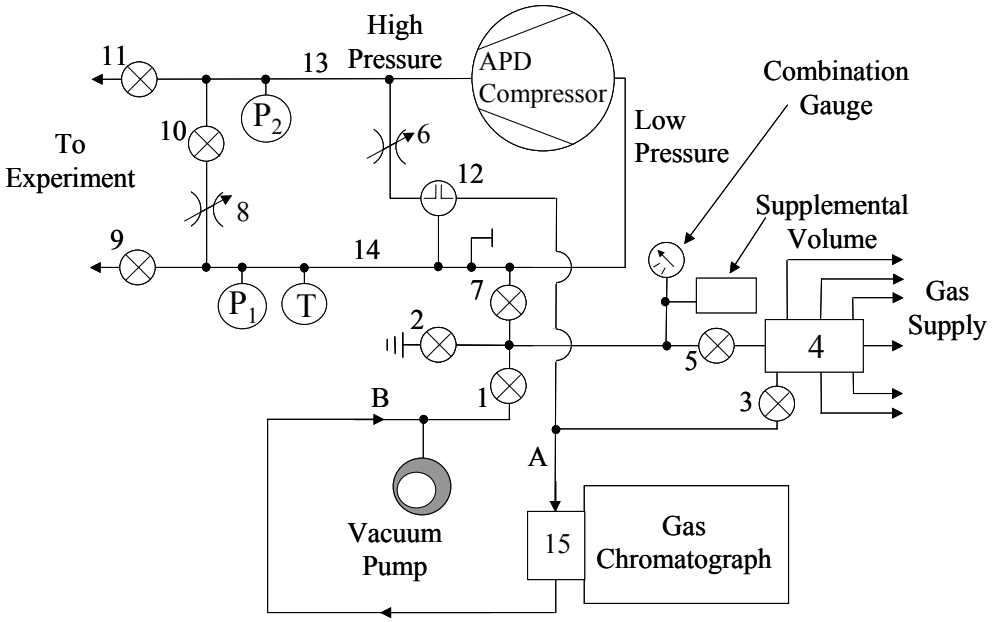

Figure 2.33. Flow Loop Schematic

Table 2.5. Flow Loop Schematic Key

Item #	Description
1	Main Vacuum Line Valve
2	Dump Line Valve
3	Manifold Vacuum Line Valve
4	Mixture Construction Manifold
5	Filling Line Valve
6	High Pressure Sample Line Throttle Valve
7	Interface Line Valve
8	Bypass Line Throttle Valve
9	Experiment Return Line Valve
10	Bypass Line Valve
11	Experiment Supply Line Valve
12	Sample Line Three-Way Selector Valve
13	High Pressure Side
14	Low Pressure Side
15	Gas Chromatograph Sampling Components
16	Sample Line Throttle Valve, see Figure X
17	Sample Vacuum Line Valve, see Figure X

2.2.4.1 APD HC-2 Compressor

A single stage APD HC-2 compressor provides steady flow to the experiment. The compressor is designed to operate with helium and serve as the compressor component of a commercial cryocooler; however, the HC-2 also operates with a charge of hydrocarbon gas mixtures. Table 2.6. lists key compressor performance specifications.

Table 2.6. Key Compressor Performance Specifications*

Maximum Pressure rise	~1800 kPa (261.1 psia)
Maximum mass flow rate	~1 g/s (2.2E-3 lbm/s)
Minimum Return pressure	~5 kPa (0.7 psia)
Heat rejection method	Water cooled
Internal Buffer Volume	Yes
Internal Bypass	Yes

*(SHI-APD Cryogenics, Inc. 2004)

Self-sealing aeroquip-type fittings connect the compressor to the flow loop. Compressor cooling water is supplied from the building water line. A solenoid valve within the compressor allows the flow of cooling water only when the compressor is operated. The waste cooling water passes to a floor drain. The compressor requires a minimum charge of approximately 930 kPa (135 psia) in order to operate. The compressor, flow loop, and test facility volumes are charged with the test fluid to a specified charge pressure. Pressure drop across the load and the initial charge pressure together determine the system operating pressures and mass flow rate. A bypass line in the flow loop allows for verification of instrumentation and compressor performance independent of the experimental facility and an adjustable throttle valve on the bypass line is capable of providing independent control of mass flow rate and operating pressures.

2.2.4.2 Flow Loop Instrumentation

The fluid temperature is measured using redundant stream penetration thermocouples at each measurement location. Each thermocouple has an uncertainty of ±1.0 K. By averaging the redundant thermocouple measurements together, the associated uncertainty is reduced to ±0.7 K. The fluid pressure is measured at the inlet and exit of the compressor with pressure transducers. The low-pressure transducer, P_1, is an Omega PX303 with a range of 0-100 psia and is accurate to within 0.25% of full scale. The high-pressure transducer, P_2, is a Setra 204 with a range of 0-250 psia and is accurate to within 0.11% of full scale. Both pressure transducers were calibrated with a dead weight tester prior to integration into the flow loop.

2.2.4.3 Gas Mixture Composition Measurement

Fluid taps placed on the inlet and exit of the compressor, shown in Figure 2.33., allow samples of the test fluid to be introduced into the gas chromatograph. A fluid sample is taken from either the high or low-pressure stream by turning a three-way valve, #12 in Figure 2.33. A throttle valve installed prior to the three-way valve on the high-pressure sampling tap reduces the pressure of the sample, #6 in Figure 2.33. Figure 2.34. is a schematic of these components, connected to the flow loop, that are used to introduce a sample into the gas chromatograph.

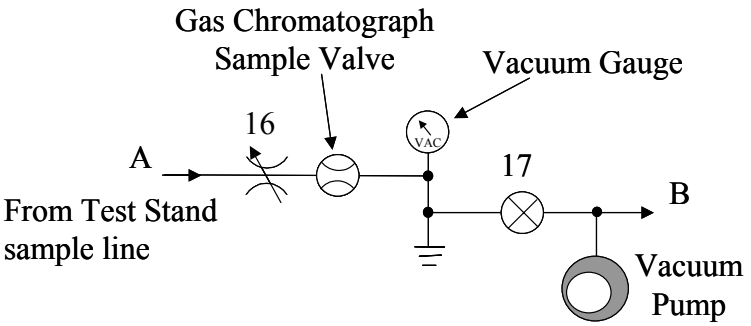

Figure 2.34. Schematic of Gas Chromatograph Sampling Components (#15 Figure X.)

A vacuum pump is used to produce a positive pressure gradient through the sampling line and remove gas from the sample line volume prior to each composition measurement.

Sampling Procedure

The procedure used to sample a gas mixture in the gas chromatograph is described below. The test facility components referred to in the procedure are shown in either Figure 2.33 or 2.34, and are listed with the assigned number in Table 2.5.

- Close the manifold vacuum line valve (3)
- Close the high-pressure sampling line throttle valve (6)
- Open the sample line throttle valve (16)
- Open the sample vacuum line valve (17)
- The sample line vacuum gauge should read approximately ¯100 kPa (gauge)
- Close the sample line throttle valve (16)
- Quickly crack (open-then-close) the high pressure sample line throttle valve (6) enough to introduce a small amount of mass into sample line

  Note: use the sound of the gas throttling across the valve as an indicator that gas is entering the sample line.

- Close the sample vacuum line valve (17)
- Slowly open the sample line throttle valve (16) and begin to introduce a sample into the sample valve
- Watch the sample line vacuum gauge, when it reaches between –20 and 0 kPa (gauge) close the sample line throttle valve (16)
- Start the GC and Integrator simultaneously (See appendix A-1 for complete GC operational procedure)

2.2.4.4 Gas Mixture Construction

Gas mixtures are constructed by charging the flow loop and test facility volumes to the specified charge pressure using the required partial pressures of the desired mixture constituents. Typical system charge pressures range from 1100 to 1300 kPa (146-174 psig). The flow loop pressure transducers successively measure the pressure of the system after each constituent is introduced. Residual gases in the system are removed prior to mixture construction with the flow loop vacuum pump. The flow loop vacuum pump is capable of pulling a rough vacuum, approximately 7.5 torr (1.0 kPa), on the flow loop.

Six high pressure gas bottles containing each of the pure constitutents provide gases to the flow loop through the mixture construction manifold which is connected to the flow loop by the filling line. The flow loop pressure transducers measure the charge pressure of each constituent during mixture construction.

Mixture Construction Procedure

- *Determine Mixture Parameters*
  - Determine the composition of the gas mixture to be run in the experiment
  - Determine the required charge pressure
  - Based on the constituent percentage and the charge, calculate the constituent partial pressure
  - The partial pressure of the constituents combined must equal the desired charge pressure
  - Mixture construction is additive, thus the pressure to which each constituent is filled, as read by the pressure transducer, is the partial pressure of the specific constituent plus the sum of the partial pressure of the constituents that preceded
  - The construction of the mixture must proceed in order of available constituent bottle pressure, where Nitrogen is the final constituent added to the mixture
- *Prepare Flow Loop*
  - Close main vacuum line valve (1)
  - Close sample vacuum line valve (17)
  - Close filling line valve (5)
  - For each bottle connected to fill manifold:
    - Close Bottle main valve
    - Close Regulator outlet throttle valve
    - Open Regulator (turn regulator actuator counter-clockwise)
  - Turn on vacuum pump

- Once pump has warmed up (est. 10-15 min), begin to slowly open main vacuum line valve (1)

  Note: keep the mass flow rate through the vacuum pump low; excessive mass flow rate is damaging to the pump and reduces the life of pump internals
- Once the pressure begins to drop in the flow loop, fully open the main vacuum line valve (1)
- Open the sample vacuum line valve (17)
- Open filling line valve (5)
- Open manifold vacuum line valve (3)
- Open Methane outlet throttle valve to view pressure on outlet combo gauge

  Note: monitor the vacuum at the constituent bottles (the furthest point from the vacuum pump) by opening the methane regulator downstream throttle valve
- Open experiment valves if an experiment is connected
- Allow enough time for the vacuum to approach ¯30 inHg on the flow loop combination gauge
- Close the filling line valve (5)
- Close the main vacuum line valve (1)

- *Constituent Charging Sequence*

  Adding the first constituent to the flow loop volume:
  - Close the manifold vacuum line valve (3)
  - Open the constituent bottle main valve
  - Open the constituent regulator outlet throttle valve
  - Set the regulator to the desired pressure

Note: pressure transducers read absolute pressure

- Open the filling line valve (5)
- Allow a reasonable amount of time for the gas to reach thermal equilibrium
- Close the filling line valve (5)
- Close the constituent bottle main valve
- Close the constituent regulator outlet throttle valve
- Open the regulator (turn regulator actuator counter-clockwise)
- Open the manifold vacuum line valve (3)
- Allow enough time for the vacuum in the manifold to approach ⁻30 inHg on the Methane bottle combination gauge
- Repeat these steps for each gas mixture constituent

- *Compressor Operation (Mixing) / Verification (GC sample)*

  Once the flow loop volume has been charged to the desired charge pressure, the mixture requires mixing. Assuming the extent of mixing among the gas constituents is a strong function of mass flow rate, the compressor is operated and the bypass line opened to allow a reasonable mass flow rate through the system.

  - Close the bypass line throttle valve (8)
  - Close the bypass line valve (10)
  - Turn on the compressor
  - Open the bypass line valve (10)
  - Slowly open the bypass line throttle valve (8) to a reasonable mass flow rate
  - Allow time for the gases to mix (~10 to 20min?)

- Sample the gas mixture and analyze with the gas chromatograph (See appendix A-1 for complete GC operational procedure)
- If the measured composition is sufficiently close to the desired mixture composition, the experiment is ready to proceed
- If the measured composition differs significantly from the desired composition, additional gas may be added during compressor operation
- To add gas during compressor operation:
    - Evacuate the manifold volume
    - Once a sufficient vacuum is established, close the manifold vacuum line valve(3)
    - Open the constituent bottle main valve and regulator outlet throttle valve
    - Set the regulator to 10 to 20 psig above the compressor suction pressure
    - Open the filling line valve (5)
    - The amount of time the filling line valve (5) is open determines the amount of constituent gas is add to the mixture

      Note: This method of mixture composition adjustment is unable to produce predictable results

3.0 Results

3.1 Test Section Verification

The test facility was designed to measure the heat transfer coefficient for a mixed-gas refrigerant; however, it is difficult to verify the accuracy of the facility based on these measurements as there exists no solid basis of comparison – no accurate predictive technique exists and there are no data available in the temperature range of interest. Therefore, the heat transfer coefficient of pure, single-phase nitrogen was measured. The behavior of single phase pure nitrogen is well understood and comparison of the measured Nusselt number to the predictions from the Dittus-Boelter correlation provides some verification of the test facility, as described in the first section. Additionally, those mixed gas data that lie in the single-phase region are also compared to the Dittus-Boelter correlation as verification of the test facility.

3.1.1 Single Phase Pure Nitrogen Tests

Figure 3.1 presents the heat transfer coefficient measurement for single phase pure nitrogen over a range of temperatures in the form of Nusselt number as a function of Reynolds number. These measurements were made at pressures from 100 to 1200 kPa, mass flow rates of 0.04 to 0.2 grams per second, and heat loads of 0.25 to 3.0 watts. The properties (viscosity and thermal conductivity) required to generate Figure 3.1 were evaluated at an average of the inlet and exit temperature and obtained using the Engineering Equation Solver software, EES. Also shown in Figure 3.1 is the Dittus-Boelter correlation for thermally and hydrodynamically fully developed turbulent flow, Eqn 3.1 (Incropera, 2002).

$$Nu = 0.023\,\mathrm{Re}^{4/5}\,\mathrm{Pr}^{0.4} \tag{3.1}$$

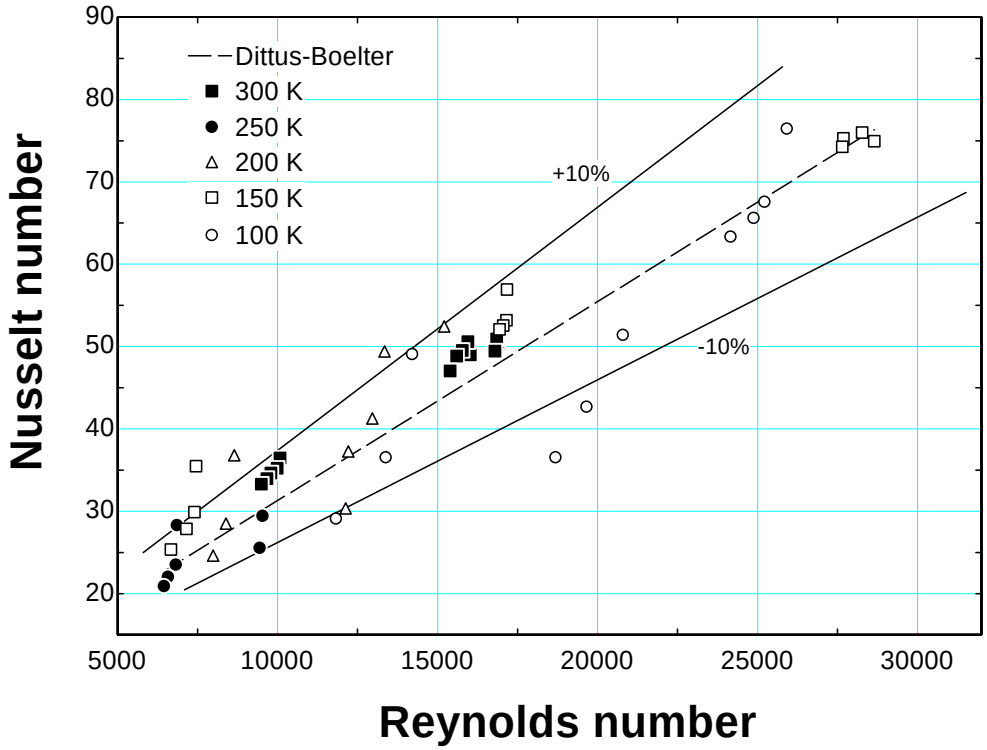

Figure 3.1. Measured Nusselt number of single phase pure nitrogen compared to the Dittus-Boelter correlation at temperatures from 300 K to 100 K

Notice that the measured Nusselt number for the single phase pure nitrogen data shows good agreement with the Dittus-Boelter correlation, typically within 10%. The measurement of the heat transfer coefficient shown in Figure 3.1 was obtained at temperatures that are representative of the intended measurement of gas mixtures, which verifies the ability of the test facility to make accurate measurement at the desired inlet conditions.

3.1.2 Single Phase Mixed Gas Tests

Some of the mixed gas heat transfer coefficient measurements presented in the subsequent section are made under single-phase conditions; these data can also be

compared to the Dittus-Boelter correlation in order to provide further verification of the test facility as shown in Figure 3.2.

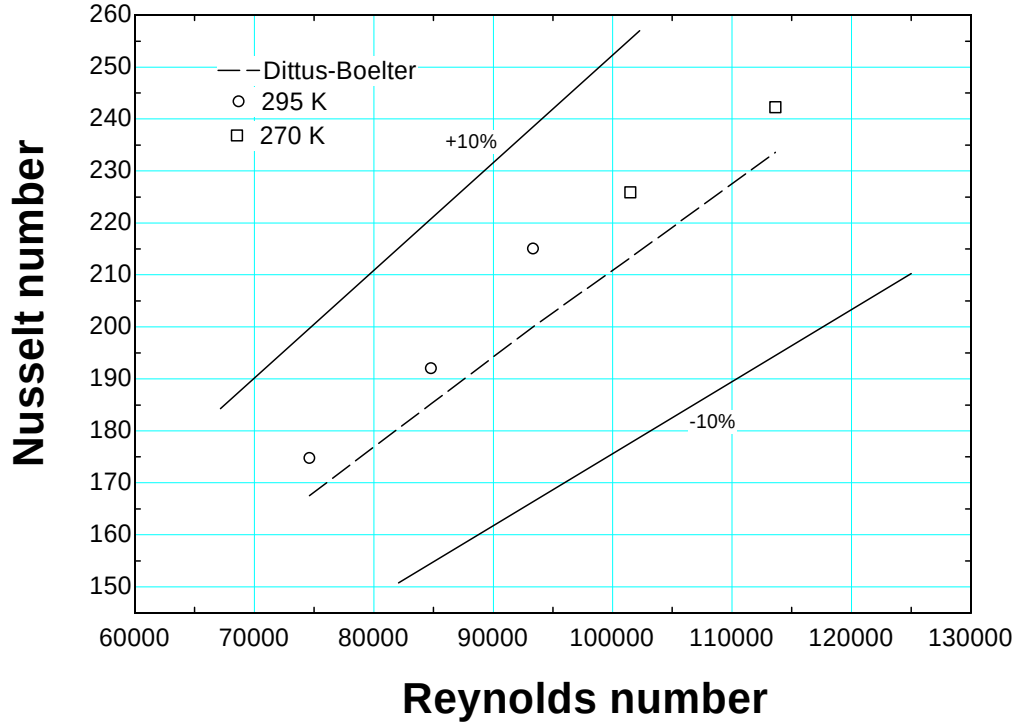

Figure 3.2. Comparison of measured Nusselt number of single phase mixed gas with the Dittus-Boelter correlation.

The agreement of the measured heat transfer coefficient with the Dittus-Boelter correlation provides further verification of the ability of the test facility to reproduce values in the known limit of turbulent single phase heat transfer, even when operating under the more complex conditions associated with a mixed-gas refrigerant.

3.2 Mixed Gas Data

This section describes the mixed-gas heat transfer coefficient data that was obtained. There were two separate tests carried out using slightly different measurement techniques. The initial measurements were taken using a stepwise measurement technique in which the test facility was sequentially changed between steady state operating conditions. These tests provided useful and accurate information about the heat

transfer coefficient but were found to be time consuming and clumsy; it was difficult to control the operating conditions in order to obtain data at a fixed value of mass flow rate, heat flux, and pressure.

Based on the results of the first tests, the test facility was modified and the test procedure was altered. Additional instrumentation and control features were added to allow a more constant mass flow rate and pressure to be achieved. Also, the test section was allowed to slowly warm up during testing in order to obtain an essentially continuous measurement of the heat transfer coefficient over the temperature range of interest.

3.2.1 Mixed Gas Test #1

This section describes the results of the initial mixed gas testing.

3.2.1.1 Measurement Procedure

The initial measurements of the heat transfer coefficient were obtained using the following procedure:

- Construct the desired gas mixture
- Turn on the compressor and energize the flow
- Open the flow to the test section
- To set the desired test section mass flow rate and pressure, adjust the needle valves:
    - at the inlet to the cryostat
    - upstream of the mass flow meter
    - on the bypass line
- Evacuate the dewar
- Turn on the GM cryocooler

- Once the test fluid reaches the desired inlet pressure, temperature and mass flow, apply the heat load to the test section
- Once the Log Mean Temperature Difference reaches steady state, record the:
    - time
    - heat load
    - volumetric flow rate
    - mixture composition, by analyzing a sample with the gas chromatograph (see appendix)
- Apply an incrementally higher heat load, when the Log Mean Temperature Difference reaches steady state, record the same measured values as listed above
- Measure the heat transfer coefficient for four or five heat loads at each inlet temperature keeping the pressure, mass flow rate, and fluid composition constant

3.2.1.2 Initial Data

Preliminary measurements were taken for a non-azeotropic hydrocarbon mixture at several values of temperatures and heat flux. The test conditions are summarized in Table 3.1.

Table 3.1: Test conditions for preliminary measurements including the theoretical uncertainty in these conditions as well as the test-to-test variation in the test conditions.

Parameter		Test Conditions	Std Deviation of Test Conditions	Measurement Uncertainty
Mass flow rate		0.65 g/s	0.12 g/s	0.03 g/s
Tube inner diameter		0.813 mm	N/A	N/A
Fluid inlet temperature		111 K to 296 K	N/A	+/- 0.18 K
Applied Heat Load		2 W to 20 W	N/A	N/A
Applied Heat Flux		29023 W/m^2 to 290234 W/m^2	N/A	N/A
Fluid inlet pressure		1069 kPa	112 kPa	2.6 kPa
Fluid Composition	Nitrogen	27.6%	4.0%	2.5%
	Methane	30.7%	2.9%	3.9%
	Ethane	7.4%	0.9%	1.0%
	Propane	32.2%	3.5%	4.6%
	Isobutane	2.3%	1.8%	0.3%

Note that the variation in the test conditions is much higher than the measurement uncertainty, which points out the problems associated with controlling the test facility. The initial measurements of heat transfer coefficient are presented in Figure 3.3 as a function of inlet temperature and in Figure 3.4 as a function of inlet quality.

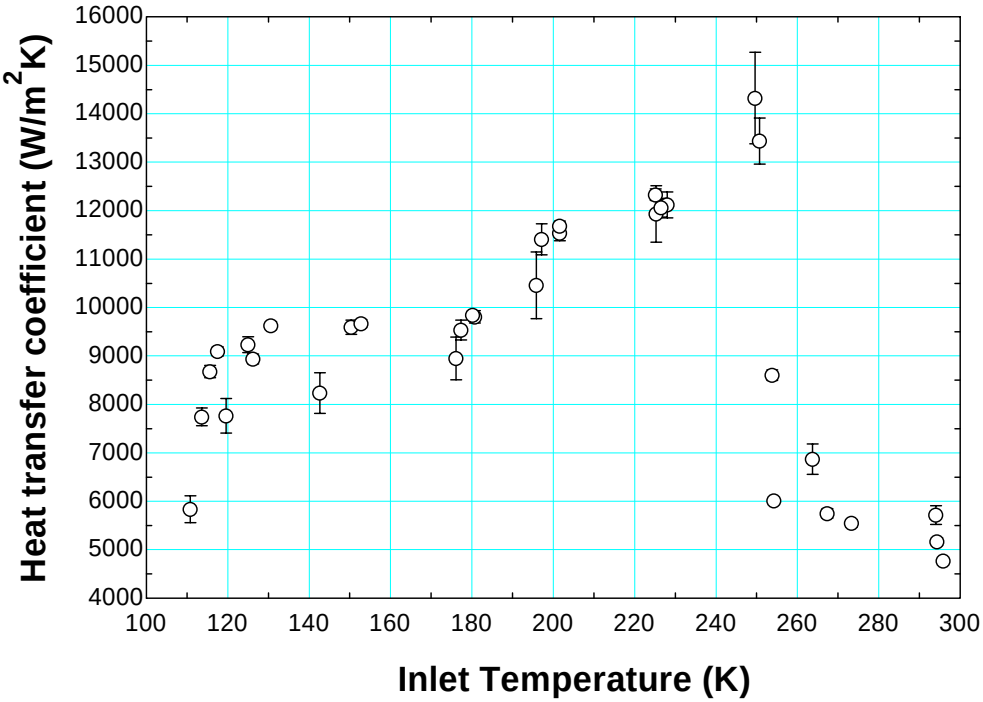

Figure 3.3. Measured heat transfer coefficient from the 1st mixed-gas tests at the conditions shown in Table 3.1 as a function of temperature

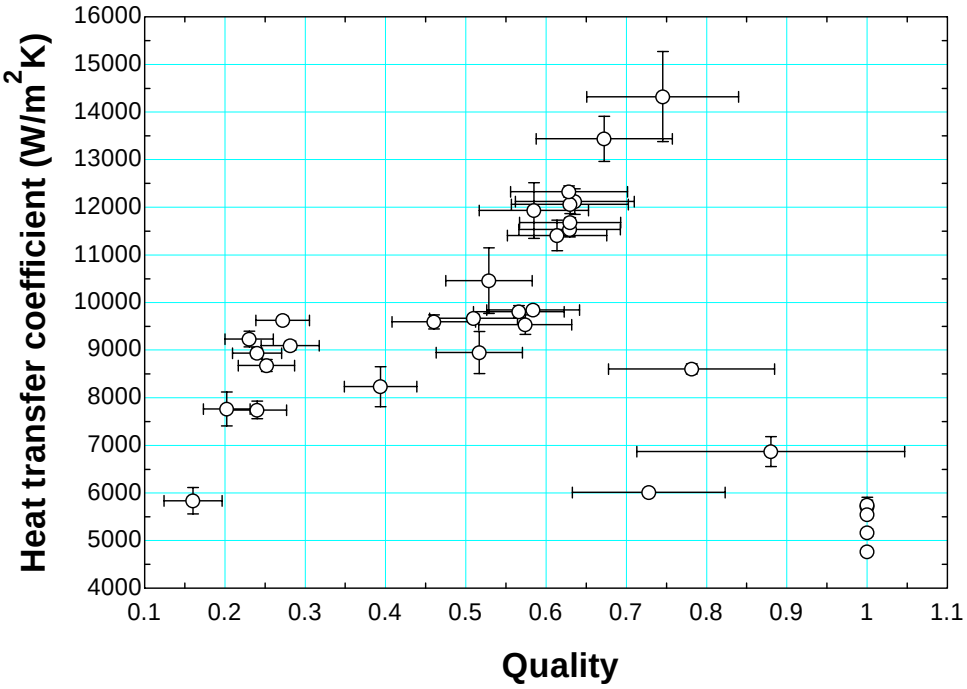

Figure 3.4. Measured heat transfer coefficient for the conditions shown in Table 3.1 as a function of quality

The rather large x-error bars in Figure 3.4 are related to the uncertainty in the composition measurements and the associated effect on the quality. Note that as the vapor quality increases, the fluid moves through several distinct modes of two-phase heat transfer:

Bubbly Flow

At vapor qualities less than approximately 0.25, small well-dispersed vapor bubbles are present in the flow. The vapor phase is sufficiently dispersed within the liquid so that it may be considered to be a homogeneous two-phase fluid. The equivalent fluid properties of a homogeneous two-phase fluid can be approximately calculated as a quality weighted average of the two-phases. The vapor phase bubbles have the effect of increasing mixing within the fluid resulting in a heat transfer coefficient that increases with quality.

Slug Flow

At a vapor quality of approximately 0.25, the dispersed vapor phase begins to coalesce into larger bubbles that have a spatial scale which is comparable to the test section diameter. These large bubbles or "slugs" of vapor intermittently create a thin annular film along the inner wall of the tube which results in a high but fluctuating heat transfer coefficient that does not change much with quality.

Annular Flow

At a vapor quality of approximately 0.55, a sufficient amount of vapor is present so that the slugs of vapor coalesce into a continuous vapor core. In this regime, a continuous annular layer of liquid exists around the circumference of the tube inner wall. The highest heat transfer coefficients are observed in this two-phase regime. Increasing vapor quality causes this annular liquid layer to thin and therefore increases the heat transfer coefficient.

Dry out

At a quality of approximately 0.75, the thin annular liquid layer begins to evaporate completely and therefore the heat transfer coefficient decreases drastically. Once dry-out occurs, the heat transfer coefficient decreases sharply with increasing vapor quality. At a vapor quality of approximately 0.90, the heat transfer coefficient approaches the value associated with the flow of a single phase vapor.

3.2.2 Mixed Gas Test #2

3.2.2.1 Facility Modification

In order to address the large variations in test section mass flow rate and pressure, shown in Table 3.1, a calorimetric mass flow meter and an inline pressure regulator were added to the test facility as shown in Figure 3.5.

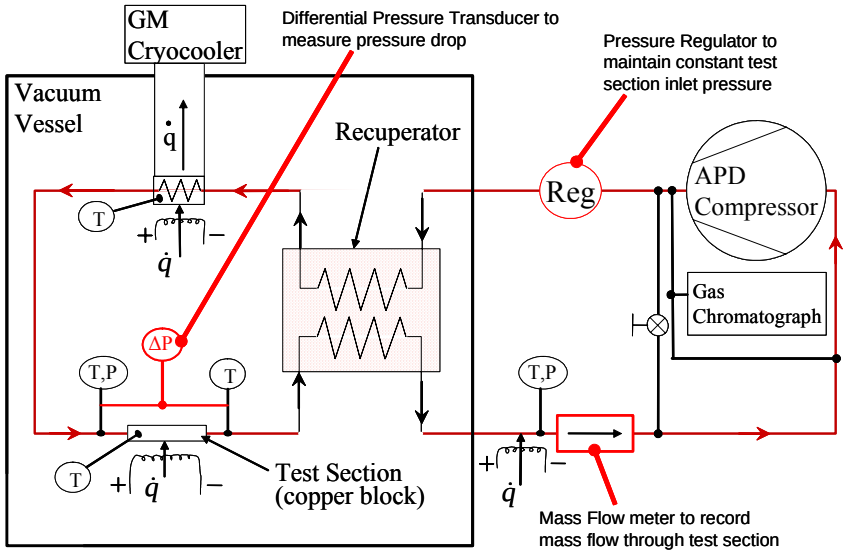

Figure 3.5. Schematic of modified test facility

The pressure regulator is used to maintain a constant operating pressure through the test section. The mass flow meter is capable of accurately measuring the mass flow rate which could be adjusted using a throttle valve placed on the outlet of the test facility.

3.2.2.2 Collection Procedure

The test facility operating procedure was changed during the 2nd mixed-gas tests. The objective was to develop a procedure that would quickly allow a complete set of data (heat transfer coefficient as a function of temperature) to be generated for a fixed set of operating conditions. During the 1st mixed gas test it was observed that the test facility required nominally 2.0 min to achieve a new steady state when the test conditions were

changed. Figure 3.6 illustrates the log mean temperature difference as a function of time and shows that the equilibration time is nominally 100 s.

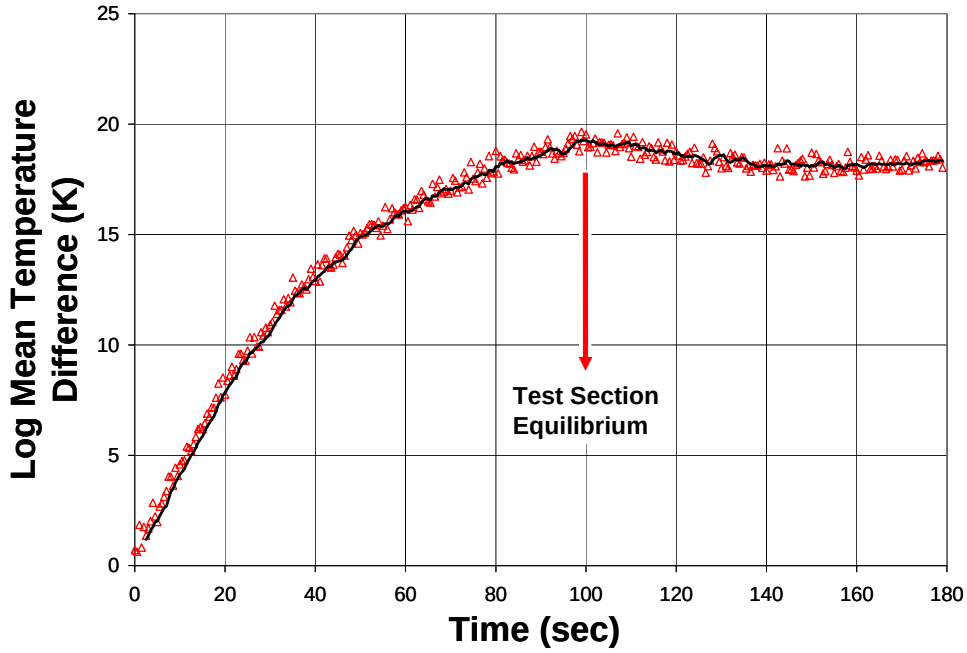

Figure 3.6. Plot of the Log Mean Temperature as a function of Time illustrating equilibration time of the test section

On the other hand, the test facility which includes the thermally massive recuperative heat exchanger and cryocooler requires nominally 250 s to change operating condition; Figure 3.7.

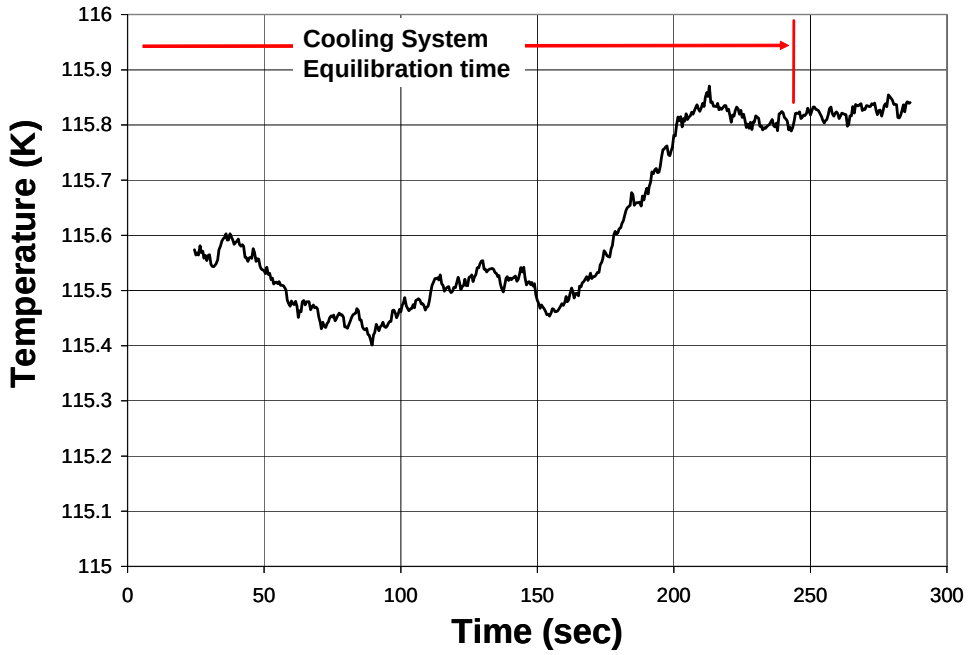

Figure 3.7. Temperature of the Cold Head of the GM cryocooler as a function of temperature illustrating the equilibration time of the cooling system

The dramatic difference between the time constant associated with the test section and the time constant associated with the test facility suggests that the test section is essentially always in a quasi-steady state as the entire test facility adjusts to changing operating conditions. Therefore, it is possible to cool the test facility to its minimum temperature and then continuously collect heat transfer coefficient data at a fixed set of operating conditions (i.e., mass flow rate, pressure, and heat flux) as the test facility warms up.

The continuous heat transfer coefficient measurement procedure is described below:

- Construct the desired gas mixture
- Turn on the compressor and energize the flow
- Open the flow to the test section
- Set the test section pressure by adjusting the pressure regulator

- Set the mass flow rate by adjusting the needle valves:
    - upstream of the mass flow meter
    - on the bypass line
- Evacuate the dewar
- Turn on the GM cryocooler
- Once the test fluid reaches the minimum inlet temperature:
    - apply a 5 Watt heat load to the test section
    - record the measured voltage and current applied to the test section
    - measure a sample with the Gas Chromatograph (see appendix..)
- After each sample has been analyzed (analyze time is approx. 30 min per sample):
    - Record the actual voltage and current applied to the test section
    - Introduce a new sample into the Gas Chromatograph
- The inlet temperature will rise as the increase in test section outlet temperature affects the inlet temperatures of the recuperative heat exchanger. Eventually the system will reach a high steady state inlet temperature. At this point, turn on and gradually increase the power to the trim heater connected to the GM cryocooler in order to slowly increase the test section inlet temperature. With the exception of the applied heat load and composition measurement, the Lab View Data Acquisition system is set up to record all the necessary data.

The transient response of the test section copper block is faster than the GM cryocooler and the associated heat exchangers, and this disparity in transient response time allows the test section to reach a quasi-steady state condition even as the inlet temperature of the

test section slowly increases; this results in a continuous measurement of heat transfer coefficient. Figure 3.8 illustrates the temperature of the test section as a function of time during the 2nd mixed gas test.

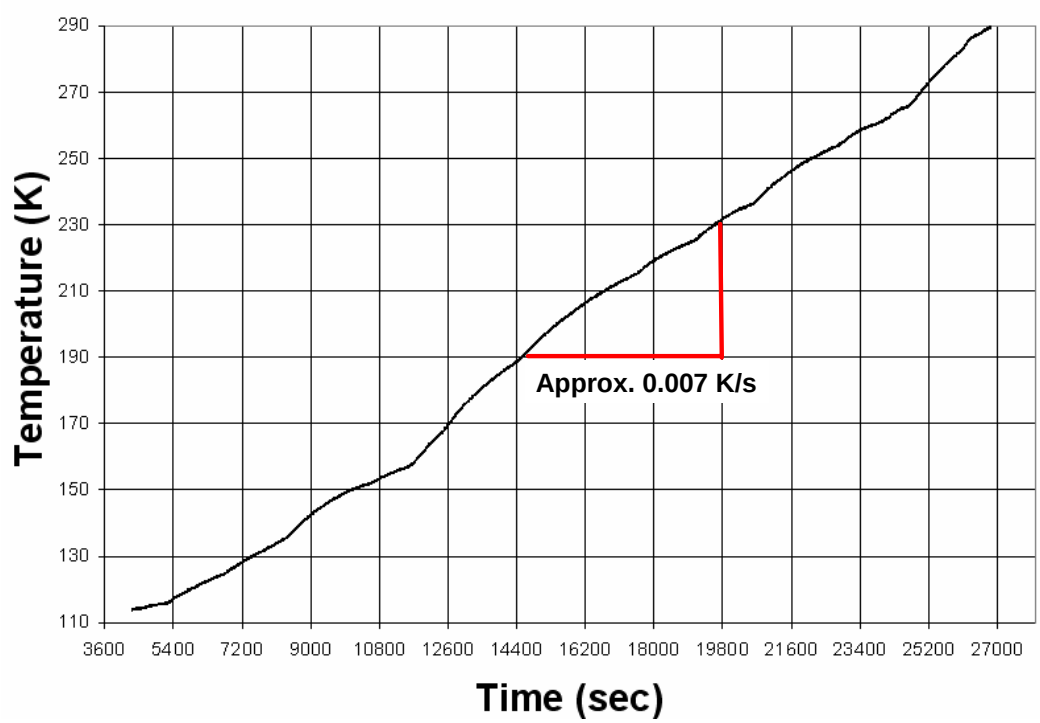

Figure 3.8. Test Section Temperature as a function of Time during the continuous measurement of heat transfer coefficient

The error in the heat transfer coefficient measurement associated with the use of the continuous test procedure as opposed to allowing the test section to achieve a true, steady-state condition before each data point can be estimated based on the time rate of change of the thermal mass associated with the test facility. Figure 3.8 illustrates that this time rate of change is nominally 0.007 K/s. The product of the temperature rate of change and the estimated heat capacity of the test section yields an error of 0.08 W; the error associated with the continuous measurement technique is less than 1% at the greatest measured heat transfer coefficient.

3.2.2.3 Continuous Heat Transfer Coefficient Data

The continuous measurement of the heat transfer coefficient was carried out for a non-azeotropic hydrocarbon mixture over a range of inlet temperatures. The test conditions used for this test are summarized in Table 3.2.

Table 3.2: Test conditions for continuous measurement including the theoretical uncertainty and variation in these test conditions

Parameter		Test Conditions	Std Deviation of Test Conditions	Measured Uncertainty
Mass flow rate		0.55 g/s	.022 g/s	0.03 g/s
Tube inner diameter		0.813 mm	N/A	N/A
Fluid inlet temperature		114 K to 290 K	N/A	+/- 0.18 K
Applied Heat Load		5.6 W	0.07 W	0.08 W
Applied Heat Flux		81265 W/m^2	1015.8 W/m^2	1161 W/m^2
Fluid inlet pressure		1340 kPa	14.5 kPa	2.6 kPa
Fluid Composition	Nitrogen	22.25%	0.7%	2.1%
	Methane	37.75%	1.1%	5.3%
	Ethane	6%	0.3%	0.8%
	Propane	34%	1.6%	4.5%

The variation of the mass flow rate and inlet pressure are reduced by nearly an order of magnitude when compared with the conditions associated with mixed gas test #1. Note that even the variation in the composition measurements are significantly reduced; the large uncertainty in the fluid composition measurement is significantly larger than the standard deviation of the fluid composition measurements.

Figure 3.9 presents a plot of the heat transfer coefficient as a function of inlet temperature at the conditions listed in Table 3.2. The values of heat transfer coefficient are consistent with the initial data set. The continuous heat transfer coefficient data also exhibits the two-phase heat transfer regimes that were evident in the initial data set. The error bars shown in Figure 3.2 indicate the associated measurement uncertainty of representative

data points. As the heat transfer coefficient increases, the associated measurement uncertainty increases. This trend is a result of the reduced temperature difference between the fluid and the tube wall for a given heat load, and is predicted by first principles as shown in Chapter 2.0.

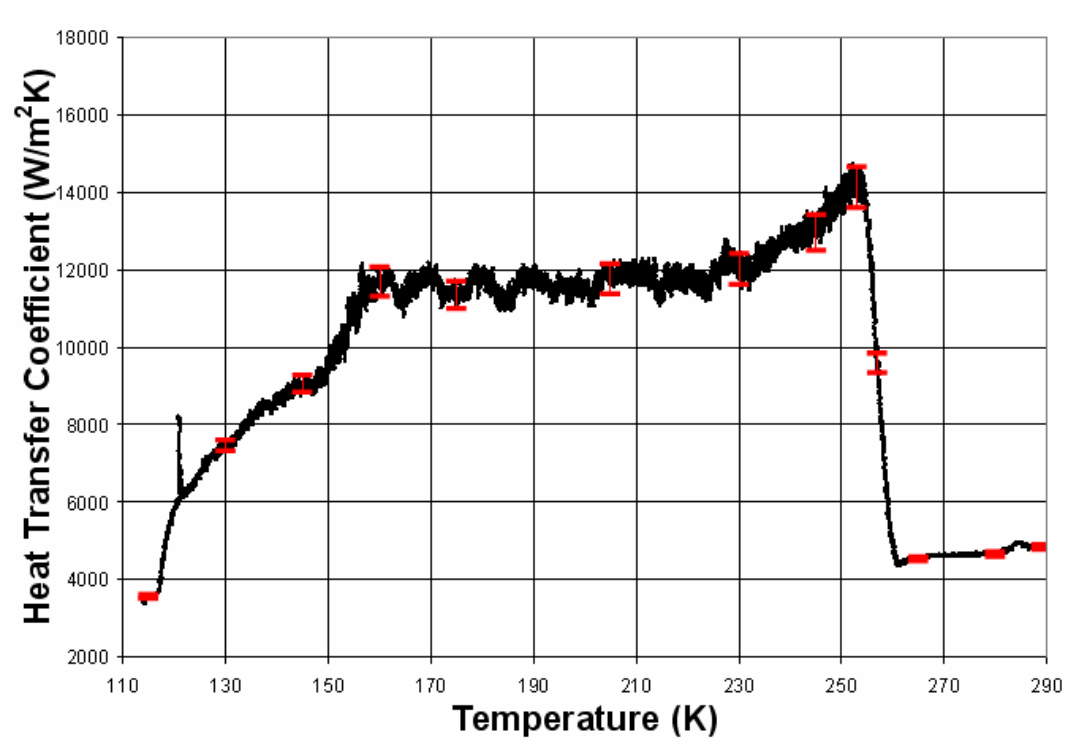

Figure 3.9. Continuously measured heat transfer coefficient for the conditions shown in Table 3.2 as a function of temperature

Figure 3.10 presents the heat transfer coefficient as a function of quality at the conditions listed in Table 3.2. The large uncertainties in the quality of the fluid are a result of the relatively large theoretical uncertainty in the fluid composition measurement. If the smaller, standard deviation in the fluid composition measurements were used, then these error bars would be reduced.

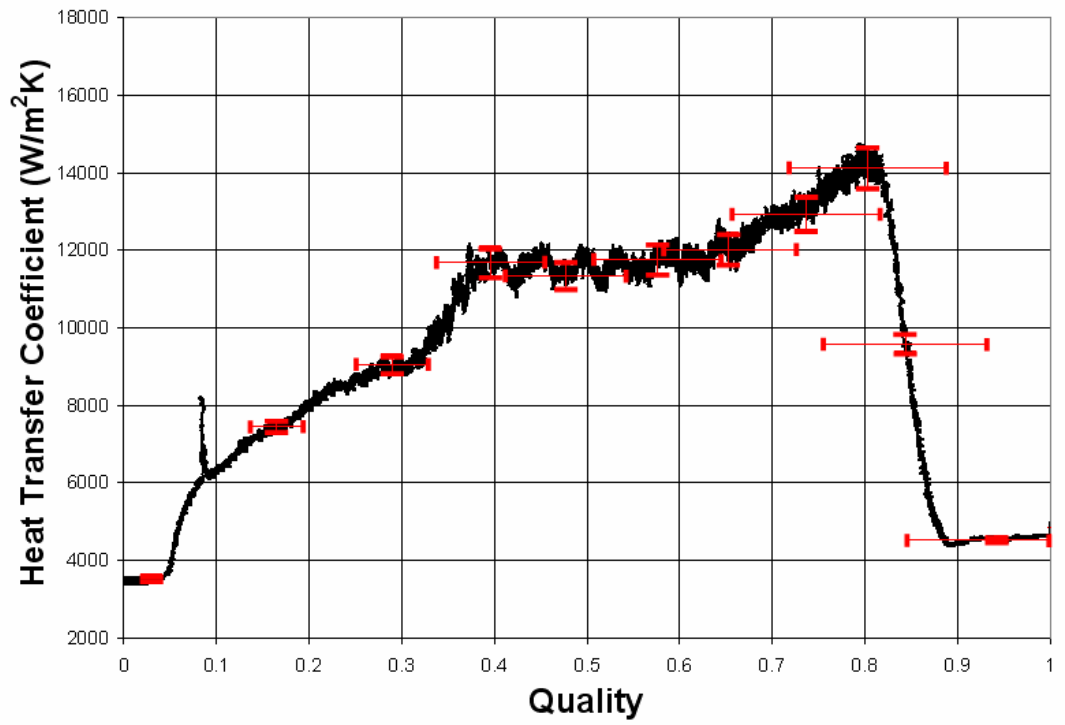

Figure 3.10. Continuously measured heat transfer coefficient at the conditions shown in Table 2 as a function of quality

Figure 3.11 illustrates the 1st and 2nd mixed gas test results overlaid upon one another. Note that these tests were carried out at different pressures and with a somewhat different mixture composition, so perfect agreement is not expected.

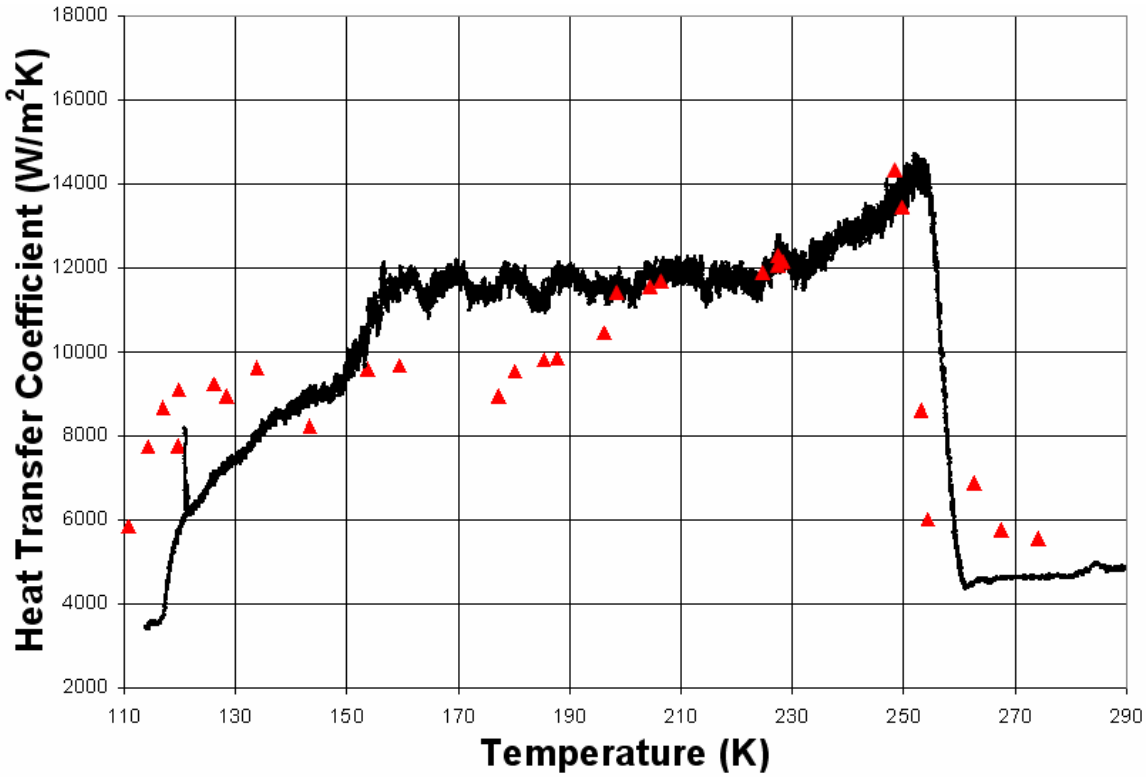

Figure 3.11. An overlay of the Heat Transfer Coefficient as a function of Temperature of the initial data on the continuous data

4.0 Conclusion

A test facility has been constructed to measure the heat transfer coefficient of non-azeotropic fluids at cryogenic temperatures. Approximation of conditions within a JT cycle recuperative heat exchanger constrained the range of test facility test conditions, and dimensions. The final design of the test facility minimizes the measurement uncertainty of the heat transfer coefficient to less than 10% for both a single phase pure fluid and single phase gas mixtures. The initial two-phase mixed gas heat transfer coefficient data corresponds to accepted two-phase heat transfer behavior. A steady state data collection method verifies the quality of the data and its value to a numerical model. An additional transient (or quasi-steady state) method of data collection providing a continuous measurement of heat transfer coefficient as a function of temperature was devised, along with facility modifications that reduce variation of the test conditions. The continuous measurement approach provides more detailed heat transfer coefficient data, such as the location of two-phase heat transfer regime boundaries. The ability of the test facility to determine the gas mixture fluid properties is limited by the large uncertainties in composition measurement.

The present work provides local heat transfer coefficients of non-azeotropic mixtures at cryogenic temperatures. These can be used, for example, in numerical models of JT cycle recuperative heat exchangers and are essential to the development of higher performance mixed gas JT cryocoolers. A search of published literature reveals a lack of relevant predictive models or empirical data. In the absence of major breakthroughs, robust predictive models of local heat transfer coefficients of two-phase non-azeotropic

mixtures are not likely to be developed in the near term. Empirical data will therefore play a central role to a greater understanding of the thermal-fluid behavior of mixed gas cryogenic refrigerants and the development of higher performance MGJT cryocoolers.

References

Alfeev, V.N., Brodyanski, V.M., Yagodin, V.M, Nikolsky, V.A., Ivantsov, A.V., 1973, "Refrigerant for a Cryogenic Throttling Unit," UK Patent 1,336,892

Boiarski, M., Khatri, A., Kovalenko, V., 1999, "Design Optimization of the Throttle-Cycle Cooler with Mixed Refrigerant," *Cryocoolers 10*, R.G. Ross, ed., Kluwer Academic/Plenum, pp.789-797.

Cryomech, 2004, "AL60," http://www.cryomech.com/products.php?item_type=p&prod_id=30&op=one

Damianides, C.A., Westwater, J.W., 1988, "Two-Phase Flow Patterns in a Compact Heat Exchanger and in Small Tubes", *Proceedings of the 2nd U.K. National Conference on Heat Transfer*, Glascow, Scotlan, vol.II, pp.1257-1268

Ely, J. F., and Huber, M. L., 2003, *NIST Thermophysical Properties of Hydrocarbon Mixtures Database (SUPERTRAPP)*, NIST Standard Reference Database 4, U.S. Department of Commerce, National Institute of Standards and Technology, Version 3.

Gong, M.Q., Wu, J.F., Luo, E.C., Qi, Y.F., Hu, Q.G., Zhou, Y., 2001, "Study on the Overall Heat Transfer Coefficient for the Tube-In-Tube Heat Exchanger used in Mixed-Gases Coolers," Advances in Cryogenic Engineering, Vol. 47A, pp.1483-1490

Incropera, F., Dewitt, D., 2002, *Introduction to Heat Transfer*, John Wiley & Sons, New York.

Jung, D.S., McLinden, M., Radermacher, R., Didion, D., 1989, "Horizontal flow boiling heat transfer experiments with a mixture of R22/R114," *International Journal of Heat and Mass Transfer*, Vol. 32, No. 1, pp. 131-145.

Kattan, N., Thome, J.R., Favrat, D., 1998, "Flow Boiling in Horizontal Tubes: Part 2 – New Heat Transfer Data for Five Refrigerants," *Journal of Heat Transfer*, Vol. 120, pp.148-155.

Keppler, F, Nellis, G., and Klein, S., 2004, "Optimization of the Composition of a Gas Mixture in a Joule-Thomson Cycle", *International Journal of Heaving, Ventilating, Air-Conditioning, and Refrigerating Research*, Vol. 10, No. 2, pp. 213-230.

Lakeshore, 2004, "PT-100 Series Platinum RTDs," http://www.lakeshore.com/temp/sen/prtd.html

Lazarek, G.M., Black, S.H., 1982, "Evaporative Heat Transfer, Pressure Drop and Critical Heat Flux in a Small Vertical Tube with R-113," *International Journal of Heat and Mass Transfer*, Vol.25, No.7, pp.945-960.

Naer, V., Rozhentsev, A., 2002, "Application of hydrocarbon mixtures in small refrigerating and cryogenic machines," *International Journal of Refrigeration*, Vol. 25, No. 6, pp. 836-847.

Rijpman, A. P., H. J. M., Holland, H. J., and Rogalla, H., 2003, "High-Tc SQUID Based Gradiometer Cooled by a Cryotiger Gas-mixture Cooler", *Cryocoolers 12*, R. G. Ross, ed., Kluwer Academic/Plenum, pp. 789-797.

SHI-APD Cryogenics, Inc., 2004, "10-K Cryocooler Compressor Options," http://www.shicryogenics.com/products/compressors.php?i=7104

Stephan, K., Abdelsalam, M., 1978, "Heat-Transfer Correlations For Natural Convection Boiling," *International Journal of Heat and Mass Transfer*, Vol.30, pp.73-87.

Stephan, K., "Heat Transfer in Boiling of Mixtures," *Proceedings of the International Heat Transfer Conference*, Munich, Paper RK14, 1982.

Wambsganss, M.W., France, D.M., Jendrzejcyk, J.A., Tran, T.N., 1993, “Boiling Heat Transfer in a Horizontal Small-Diameter Tube,” *Journal of Heat Transfer*, Vol. 115, pp.963-972.

Zhao, Y., 2001, *Flow Boiling Charactersitics Of Carbon Dioxide In Microchannels*, Ph.D. Dissertation, University of Maryland.

Appendix

A-1 Gas Chromatograph Procedure

General Procedure

1. Turn on GC at the lower right hand corner
2. Initiate carrier gas flow at helium cylinder
   - set to around 75 psig
3. Set Oven Temperature [OVEN TEMP] value [ENTER] to 35 C
4. Set Injection and Detector Temperature at 150 C each.
5. Allow oven to reach temperature
6. Set flow rates: Use GC's stop watch 3x[TIME] and attach bubble flow meter to rubber hose coming out of GC top door. Close reference needle valve by rotating black knob clockwise. Push [ENTER] and squeeze bulb simultaneously. Once bubble reaches 10 push [ENTER]1/t value*10= mL/min. This is carrier rate. Open reference valve to view sum of carrier and reference rate. Vary flow with both delivery pressure helium cylinder regulator and carrier and reference flow valves. The reference needle valve is adjusted with the the tiny screw inside of the black knob.
   - carrier 25 mL/min, reference 50 mL/min
7. Allow enough time for flow conditions to be constant throughout column.
8. Turn on Detector [Det] [ON] [ENTER]
9. Set Detector to low sensitivity while signal equilibrates. [GOLD] [DET] [OFF]
10. Assign signal to Detector [Sig 1] [A] [ENTER] and watch signal by pressing [SIG 1] again.
11. Once signal is around 4.5 , turn back on High Sensitivity to evaluate rate that signal is dropping. [GOLD] [DET] [ON]
12. When sample has been introduced into sample valve, Push [START] on the GC and integrator simultaneously,

Table 1. lists the retention times for the gases used, at the oven temperatures specified previously. The retention time represents the time it takes for the gas to travel through the column and be detected.

Table 1. Approximate Gas Retention times at the oven temperature program used [35 C for 7.5 min, 50 C/min ramp, 220 C for 12.8 min]

Gas	Nitrogen	Methane	Ethane	Propane	Butane
Retention Time (min)	3.1	5.8	13.5	17.3	22.7

Stand-By

1. Turn Detector on Low sensitivity and leave everything else.

Shut Down

1. Set Temperatures to 27 C
2. Once column has cooled close to room temperature, end carrier flow at cylinder, do not disturn carrier and reference valves
3. Turn off detector. DET [OFF]
4. Once temperatures have reached room temp, turn off GC. Leave integrator on

A-2 Uncertainty Analysis of Gas Chromatograph (Alex Dodd, 5/14/04)

There is a certain amount of variation in the results of each test run of the Gas Chromatograph (GC). While determining the chromatograph's sensitivity to each type of gas, and performing tests on mixture compositions, this variation propagates uncertainty. By finding the variation in measurement of each pure type of gas and accounting for a possible discrepancy in bottle purities of each type of gas, an uncertainty in multiplication factors was determined. Even though gas chromatograph readings vary significantly each day, the daily variation in multiplication factor (MF) remains within this range. Therefore, the uncertainty in multiplication factors was confidently assigned a conservative estimate of ten percent. Then, by investigating the variation in reported areas while analyzing a gas mixture, a coefficient of variation (Standard Deviation of Sample Areas/Mean Area) for each gas was found. Because of the relative similarity in these values between gas types, a conservative value of seven percent for the coefficient of variation of all gas types has been assigned.

When testing each pure gas sample and one mixture sample twelve times in one period, very optimistic uncertainty values were found. However, this procedure lasts close to twenty-four hours. Therefore, by assigning the aforementioned conservative values, acceptable values of composition uncertainty can be obtained by simply analyzing mixtures. In some cases, outliers did occur; therefore, it is recommended to assure mixture compositions by performing a few runs.

Both of these assigned uncertainties propagate to provide an uncertainty in composition percentage in each gas. A program and diagram window, (GC_Uncertainty.EES), has been created to calculate this final uncertainty based on mixture areas. If different GC Oven Temperatures, gas flow rates, or gas cylinders are desired, new multiplication factors should be calculated by obtaining the mean of five pure samples and inserting them as "Gaspure" variables. The assigned variations remain valid with different MF values.

Table 1 shows a synopsis of all final results. "Reported" values are those returned from an analysis performed during continuous operation with sample sizes of twelve and a confidence level of 95% (Appendix 1) while "Assigned" values are those recommended to be used for future mixture analysis. All values are meant for the case of a mixture containing Nitrogen, Methane, Ethane, Propane, and Butane where Nitrogen and Methane enter the detector during an Oven Temperature of 35^{o} C and the other hydrocarbons enter the detector at 220^{o} C. Also in this case, the carrier and reference gas flow are set at 25 and 50 mL/min respectively while the oven temperature is set at 35^{o} C.

Table 1: Summation of Gas Chromatograph Precision

Gas Type	Nitrogen	Methane	Ethane	Propane	Butane
Recommended MF value	1	1.26	0.599	0.509	0.431
Reported Uncertainty in MF	0.000	0.094	0.057	0.048	0.031
Assigned Uncertainty in MF	0.000	0.126	0.059	0.051	0.043
Reported Coef. Of Var. in Mix Area (%)	6.57	3.41	2.61	3.92	5.85
Assigned Coef. Of Var. in Mix Area (%)	7	7	7	7	7
Reported Composition (%)	27.13	26.72	15.94	26.42	3.86
Composition Uncertainty, Reported Values (%)	2.16	2.51	1.74	3.37	0.39
Composition Uncertainty, Assigned Values (%)	2.39	3.56	2.13	3.52	0.51
Uncertainty in Comp. w/ equal proportions (20% of each gas), from Assigned Values (%)	1.731	2.649	2.646	2.643	2.636

Introduction

Because of the method used to perform gas mixture analysis with the chromatograph located in the SEL, the uncertainty is caused by impurity in the gases used for calibration and a variation in the chromatograph readings. Once an understanding of the procedure used to find mixture composition is understood, an uncertainty analysis can be performed.

Procedure to Determine Composition and Subsequent Uncertainty

A thermal conductivity detector has varying sensitivity to each gas. Determination of the detector sensitivity, relative to a pure gas sample, allows for the correct measurement of a mixture composition. A Multiplication Factor, equal to the ratio of the pure gas area response to the pure nitrogen area response, compensates for different sensitivities. To measure a mixture composition, each peak's area is multiplied by its appropriate multiplication factor to obtain a "corrected area". The "corrected areas" are then divided by the "total corrected area" to determine each constituent percentage.

1 Pure Gas Calibration Runs

Performing a calibration prior to the measurement of a mixture composition effectively eliminates variations in GC readings. Calibration consists of obtaining an area for the pure form of each mixture constituent.

The uncertainty in the "pure area" value is the standard deviation of the returned pure values. Within one day, standard deviation (S_x) and mean ($\overline{x}$) values for a sample size of twelve were obtained (Appendix 1). On other days, the same data was obtained for a sample size of ten (Appendix 2). In all tests, each pure gas type maintained a coefficient of variation of less than 4% before accounting for applying finite statistical methods.

While injecting pure samples of hydrocarbons, a small peak with a retention time similar to Nitrogen occurs. Some of this peak is impurities in the hydrocarbon bottles. However, this peak gains in size according to the amount of time between filling the sample line and sample injection. Because the sample line is below atmospheric pressure, this

suggests an air leak in the sample line. No leaks were detected in this line with the helium leak tester. The effect of this peak on sample data is basically negligible. Even though, it should be common practice to quickly inject samples once the sample line has been filled (Appendix 2).

Finite Statistical Method

The standard deviation describes an interval in which all values are expected to lie. However, since this standard deviation is found through a finite number of measurements, it is possible that all of the characteristics of the chromatograph readings may not be contained in the data set. Therefore, the standard deviation must be multiplied by a value (student-t value, $t_{student}$) in order to inflate the interval to contain more of all possible values.

$$Interval\ Limits = \overline{x} \pm t_{student} * S_x$$

This value is determined according to the theoretical normal distribution of data. No extensive tests were performed to assure that the chromatograph's data is normally distributed, however, nothing has indicated otherwise. More data characteristics are expected to be accounted for as sample size approaches infinity. It is recommended that for sample sizes less than or equal to 10, sample statistics can be misleading. Therefore, for a given variance (number of samples-1), a table of Student-t distribution values gives the necessary inflation of the interval in order to contain all points to within a given probability. The probability that all data points will fall within this interval is called the confidence level. Table 2 shows the change in student-t distribution with sample size and confidence levels.

Table 2: Student-t Distribution

Sample size (N)	Student-t Values for Given Confidence Levels			
	50%	90%	95%	99%
2	1.000	6.314	12.706	63.657
5	0.741	2.132	2.770	4.604
10	0.703	1.833	2.262	3.250
12	0.697	1.796	2.201*	3.106
20	0.688	1.729	2.093	2.861
31	0.683	1.697	2.042	2.750
Infinity	0.674	1.645	1.960	2.576

*****Value used for calculations

Other uncertainty in the multiplication factor arises when one realizes that the calibration samples are not actually pure gases. Each of the pure gases used actually has an assigned purity with a corresponding uncertainty. Proper calculation of this MF must include the constituent purity. In most cases, the difference in results from this realization is negligible. However, if this were not accounted for, the MF would gain significant uncertainty while testing bottles with a significant difference in purity. Therefore, the

"intermediary area" value used to calculate the MF is the "pure area" divided by the specified purity.

Intermediary Area (intA) = Pure Area (pureA)/gas purity

The uncertainty in this "intermediary area" is dependent on both the variation in the "pure area" and the uncertainty in the accuracy of each gas. Steps for calculating the total uncertainty in the "intermediary area" of a specified gas are as follows:

$$\frac{\partial \text{int } A}{\partial pure\ A} = \frac{1}{gas\ purity}$$

$$\frac{\partial \text{int } A}{\partial gas\ purity} = \frac{pure\ A}{\left(gas\ purity\right)^2}$$

$$\sigma_{\text{int } A} = \sqrt{\left(\frac{\partial \text{int } A}{\partial pure\ A} * StdDev\ of\ Pure\ A\right)^2 + \left(\frac{\partial \text{int } A}{\partial gas\ purity} * Accuracy\ of\ Gas\ Purity\right)^2}$$

2 Calculating Multiplication Factor

The multiplication factor is calculated as:

$$Multiplication\ Factor\left(MF\right) = \frac{\text{intermediary } area\ of\ nitrogen\left(N_2 A\right)}{\text{intermediary } area\ of\ specific\ gas\left(gas\ A\right)}$$

MF variation from run to run:

The uncertainty in each multiplication factor is:

$$\frac{\partial MF}{\partial N_2 A} = \frac{1}{gas\ A}$$

$$\frac{\partial MF}{\partial gas\ A} = \frac{N_2 A}{\left(gas\ A\right)^2}$$

$$\sigma_{MF} = \sqrt{\left(\frac{\partial MF}{\partial N_2 A}\left(\sigma_{\text{int } A of\ N_2}\right)\right)^2 + \left(\frac{\partial MF}{\partial gas\ A}\left(\sigma_{\text{int } A of\ gas}\right)\right)^2}$$

Since the multiplication factor for nitrogen is assigned at 1, the subsequent uncertainty is zero. The suggested multiplication factor is based on the aforementioned standard deviation calculation of twelve runs (Appendix 1). The uncertainty in the multiplication factor was then taken as the greater of the two differences between the mean and interval bounds. Table 3 provides a synopsis of these results.

Table 3. Results of Multiplication Factor

	Methane	Ethane	Propane	Butane
MF Mean	1.26	0.599	0.509	0.431
Uncertainty	.0942	.0571	.0480	.0311

Because tests with Ethane, Propane, and Butane are performed at a different oven temperature than Nitrogen, their multiplication factor will change if tests are ran at different oven temperatures than suggested. This change in multiplication factor results from a decrease in carrier gas flow rate at higher temperatures; because the ratio of carrier gas flow to reference gas flow rate changes, the detector sensitivity is affected. It is now suggested that Nitrogen and Methane are ran at 35^{o} C and the other hydrocarbons have an oven temperature of 220^{o} C.

The results of Table 3 suggest that the uncertainty in multiplication factor be assigned at 10%.

MF Variation from day to day:

The raw area calculations of the chromatograph vary significantly from day to day. Suspected sources of this variation are contaminants entering the column and detector during shutdown, and change in the ratio between carrier and reference gas flow rate. Because of this variation, it is necessary to estimate the daily variation in the multiplication factor. Past data was analyzed to prove that the multiplication factor remains within the expected interval from day to day. Although data on Propane and Ethane was taken at a different Oven Temperature rather than the currently recommended Oven Temperature, it can be seen that the daily variation between multiplication factor calculations remains within the expected interval. Furthermore, the mean value of all Methane multiplication factors is nearly equal to the suggested multiplication factor.

Table 4: Similarity in Multiplication Factor Data from Day to Day (Oven Temp, N2 and Methane 35 C, Ethane and Propane 190 C)

Date	# of samples	Methane	Ethane	Propane
1/8/2004	3	1.386		
1/11/2004	3	1.301		
1/13/2004	3	1.204		
1/14/2004	1	1.237		
1/16/2004	2	1.165	0.605	0.633
1/21/2004	1	1.223	0.608	0.481*
1/18/2004	2		0.700	0.678
2/20/2004	10			0.6051
Mean		1.253	0.638	0.618
Standard Deviation		0.079	0.054	0.085
Coef of Variation (%)		6.324	8.443	13.709

*suspected outlier, but included in calculations

After realizing the day to day characteristics of the multiplication factor are similar to the run to run characteristics, an uncertainty of 10% can confidently be assigned. However, it is common practice with gas chromatographs to recalibrate when new tanks of gas are

used. A change in carrier gas purity or the ratio of purities between sample gas cylinders could seriously affect multiplication factors. **Therefore, it is recommended to find new multiplication factors when the following events occur:**

- New helium tank for carrier/reference gas flow
- Any new gas tanks
- Test runs performed at different temperatures than 35 C for Nitrogen and Methane and 220 C for Propane, Methane, and Butane.

When gases enter the detector after an Oven Temperature Ramp, the same ramp must be used to find their "pure areas" in order to obtain accurate results (Appendix 4). However, the exact same Oven Temperature program isn't necessary. For the case of hydrocarbons entering the detector at 220^{o} C, the same ramp as used for mixture analysis began at 35^{o} C after one minute.

3 Performing Mixture Analysis

Once the Multiplication Factors of each gas are found, a mixture containing those gases can be analyzed. When this is done however, there is variation in the area output of each peak. This is termed the "Mixture Area" and its correlating variation is the "standard deviation of the mixture area." For each of the Nitrogen/Hydrocarbon mixture possibilities, this standard deviation has been found using a sample size of twelve and a confidence level of 95%. After repeated testing, it is shown that the standard deviation of each peak is correlated to its mean value. Therefore, the variation of the "mixture area" is characterized by its coefficient of variation. Between all "mixture areas" for each type of gas, coefficients of variations have remained below 7%. Therefore, a conservative value of 7% has been assigned to each gas type's coefficient of variation. In the program GC Uncertainty.EES, the "Mixture Areas" entered in the diagram window are multiplied by this value to obtain an appropriate standard deviation for uncertainty calculations.

4 Finding the Correct Area

As stated before, the "mixture area" must be multiplied by its appropriate multiplication factor in order to find its "correct area." Therefore, the uncertainty these "correct area" values is determined by both the standard deviation of the "mixture area" and the uncertainty in the multiplication factor. The equations for finding the uncertainty in the correct area are as follows:

$$\sigma_{Correct\ Area} = \sqrt{\left(\frac{\partial Correct\ Area}{\partial MF}\left(\sigma_{MF}\right)\right)^2 + \left(\frac{\partial Correct\ Area}{\partial Gas_{mix}}\left(\sigma_{Gas_{mix}}\right)\right)^2}$$

$$\frac{\partial Correct\ Area}{\partial MF} = MF$$

$$\frac{\partial Correct\ Area}{\partial Gas_{mix}} = Gas_{mix}$$

5 Finding the Composition:

Once the correct areas are found, the composition may be calculated. This is achieved by adding up all the correct areas to obtain a "Total Area." Then for each gas, the correct area is divided by this total area and multiplied by 100 to obtain the composition of each gas in percentage form:

$$\text{Composition (Comp)} = \frac{Correct\ Area}{Total\ Area} * 100$$

For a mixture containing nitrogen and n number of other gases:

$$\sigma_{Total\ Area} = \sqrt{\sigma_{N_2}{}^2 + \sigma_{Gas1}{}^2 + ...\sigma_{Gas(n)}{}^2}$$

Therefore the uncertainty in composition is as follows:

$$\sigma_{Comp} = \sqrt{(\frac{\partial Comp}{\partial Area\,Total}\sigma_{Total\ Area})^2 + (\frac{\partial Comp}{\partial Correct\ Area}\sigma_{Correct\ Area})^2}$$

$$\frac{\partial Comp}{\partial Total\ Area} = \frac{Correct\ Area * 100}{Total\ Area^2}$$

$$\frac{\partial Comp}{\partial Correct\ Area} = \frac{100}{Total\ Area}$$

Conclusion

By finding multiplication factors and analyzing a mixture with a large sample size in one day, it was shown that the precision of the gas chromatograph allows for adequate accuracy in the estimation of gas mixture composition. From this data, conservative estimates of the variation in multiplication factor (10 %) and the coefficient of variation of mixture areas (7%) were assigned. While being conservative, these values still allow for adequate accuracy. Then, by comparing the multiplication factor found with this large sample size to previous multiplication factor calculations, it was found that the multiplication factor remains relatively constant given similar run conditions, allowing the avoidance of calibration on a day to day basis.

Currently, composition uncertainties will range from .5 to 5 % depending on composition percentages. If a more accurate analysis is ever needed, this chromatograph has the capabilities. A large source of error is the lack of human precision while introducing a sample. This could be avoided by attaching a precision regulator directly before the sample line, constraining sample pressure to within the limits of the regulator.
Also, accuracy could be improved by completely sealing the sample line. However, the effects of this leak are nearly negligible if the sample is injected quickly after being introduced into the sample line.

During analysis, outliers occurred on occasion. These would usually occur in the beginning of GC operation. Therefore, it is recommended to analyze well-mixed mixtures more than once to ensure composition estimations. Suggested GC operation parameters are included in the Diagram Window of the EES program "GC.Uncertainty." If these parameters are followed, the program will calculate composition and uncertainty correctly. If parameters are changed, it is recommended to run each pure gas at the new parameters five times and enter the mean value into the "Gaspure" variables. Then the program will successfully calculate values based on a more accurate multiplication factor. If smaller uncertainty values are ever desired and more tests are performed, test values may be entered into this program to find major sources of uncertainty.